2017

Multiscale Modeling of Carbon Nanotube Synthesis in a Catalytic Chemical Vapor Deposition Reactor

Jonathan Troville
Wright State University

MULTISCALE MODELING OF CARBON NANOTUBE SYNTHESIS IN A CATALYTIC CHEMICAL VAPOR DEPOSITION REACTOR

A thesis submitted in partial fulfillment of the
requirements for the degree of
Master of Science

By

JONATHAN TROVILLE
B.S., PURDUE UNIVERSITY, 2015

2017
Wright State University

Wright State University
GRADUATE SCHOOL

April 28,2017

I HEREBY RECOMMEND THAT THE THESIS PREPARED UNDER MY SUPERVISION BY Jonathan Troville ENTITLED Multiscale Modeling of Carbon Nanotube Synthesis in a Catalytic Chemical Vapor Deposition Reactor BE ACCEPTED IN PARTIAL FULFILLMENT OF THE REQUIREMENTS FOR THE DEGREE OF Master of Science.

Prof. Amit Sharma
Thesis Advisor

Prof. Jason Deibel
Chair, Department of Physics

Committee on Final Examination

Prof. Gregory Kozlowski

Prof. Brent Foy

Prof. Amit Sharma

Robert E.W.Fyffe, Ph.D.
Vice President for Research and
Dean of the Graduate School

Abstract

Troville, Jonathan. M.S. Department of Physics, Wright State University, 2017. Multiscale Modeling of Carbon Nanotube Synthesis in Chemical Vapour Deposition Reactor.

The bottom-up analysis of Carbon Nanotube synthesis is not well understood. Specifically, the question as to how carbon adsorbs to a substrate inclusive of a supported catalyst may lead to the energetically favorable structure of a hexagonal close-packed structure along the wall, or walls, of the tube. A first time simulation using COMSOL Multiphysics has been generated in order to capture the gas-phase mechanism which leads to carbon production. It is thought that the carbon adsorbs and the walls are formed from the bottom up and the inside out for multi-wall CNTs. The studies involved accurately setting up a simulation to capture chemical kinetics, mass transport, heat transfer, and fluid flow.

It is shown that a variation in inflow velocity yields a variation in efficiency of ethylene cracking in the reactor. When the residence time is increased the outlet concentration of ethylene is lowered, as expected. This means that variations in concentrations can be accounted for through varying initial parameters.

Chemical reactions involving ethylene decomposition from GRI-Mech 3.0 [4] is imported and the validity of the Troe Form chemical kinetics was tested. Using equilibrium calculations with the use of an ICE (Initial, Concentration, Equilibrium) table, 0-D studies using the high pressure limit of the rate constant and the Troe

Form of the rate constant were used in separate tests for comparison. It was subsequently showed that the Troe Form kinetics do not accurately determine the expected concentrations.

The chemical species concentration, gas pressure, temperature, and velocities were calculated for a final set of approximately 32 gas-phase reactions. A nearly completed set of gas-phase and surface reactions were compiled but only the most important chemical reactions were implemented in the present studies to form a basis for future analysis. The results of the present study shows production of amorphous carbon within the gas-phase, which is not high enough for CNT growth, implying the importance of surface hydrocarbon reactions in the CNT production in a CVD reactor.

Contents

List of Figures

Page

List of Tables

Page

Acknowledgements

I want to thank Dr. Amit Sharma for the endless support and guidance, Dr. Ahmad E. Islam for guided support at Wright Patterson AFB, and Dr. Benji Maruyama for the great experience to work in his research group.

Dedication

I would like to dedicate this to my lovely wife who has been very supportive through the entire research process.

Chapter 1

Introduction

A Carbon Nanotube (CNT) is a folded, hollow, cylindrical structure of carbon atoms which can also be viewed as a structure formed by the folding of a graphene sheet – a monolayer of carbon atoms which are bonded in a hexagonal, honeycomb lattice [6]. There are infinitely many ways to roll a sheet into a cylinder, thus resulting in CNTs of different diameters and microstructures. A tube made of a single graphene sheet is called a Single-Walled Nanotube (SWNT), whereas a tube comprising of several concentrically arranged cylinders is referred to as a multiwall tube (MWNT) [6]. Research on CNTs has grown exponentially within the last decade and great progress has been made toward both theoretical and experimental studies including synthesis and applications. CNT production capacity has increased 10-fold resulting in large growth of CNT-related commercial activity ranging from rechargeable batteries, automotive parts, water filters, with promising future applications including supercapacitors, actuators and lightweight electromagnetic shields [6]. Leveraging CNT dispersion, functionalization, and large-area deposition techniques, CNTs are also emerging as a multifunctional coating material.

At present there are several ways to produce CNTs; arc-discharge, laser ablation, chemical vapor deposition (thermal, plasma, laser assisted, and catalytic) and flame synthesis to list a few established methods [6]. Each method has its strengths and weaknesses with abundant literature on each of these methods and therefore we do not provide further details in this thesis. However, we provide a brief description of the Chemical Vapor Deposition (CVD) process which has direct relevance to the work performed under the current project.

1.1 Chemical Vapor Deposition Reactor

Chemical vapor deposition synthesis of CNT can be understood as a chemical process in which a volatile precursor (such as ethylene) is injected into a reaction chamber to provide a carbon feed. A catalyst particle or substrate is maintained at an elevated temperature in the reaction chamber. The precursor undergoes chemical decomposition and CNT is grown on the aforementioned (metal) catalyst. This approach is a multivariable process and can be adjusted in several manners to grow CNT with desired structural properties. In a CVD reaction the catalyst particles can also reside in free space (floating catalyst) or catalyst particles can be formed by the decomposition of a volatile metal-containing precursor as for a carbon source.

The growth mechanism of CNT on a supported catalyst is largely unknown due to the large number of chemical reactions that occur during the growth process – starting with the decomposition of the carbon precursor and the end process of CNT growth on catalyst metals. It has been proposed that the growth of CNT is comprised of two major steps: 1) initial cap formation (nucleation), and, 2) addition of carbon along the circumference (growth). The formation of closed cap is also supported by ab-initio calculations which show that the nucleation of a closed cap is energetically favorable compared to any structure with dangling bonds or to a fullerene. Experimental observation also points to the mechanisms of bulk diffusion and surface diffusion as possible mechanisms of addition of carbon atoms to the base of nanocap.

Figure 1.1 displays the aforementioned process. Species from gas-phase reactions are thought to adsorb to the surface of the supported substrate. In order for the CVD process to occur, a buffer gas (stagnant gas in Figure 1.1) is flown into the reactor chamber. This allows for pressure-dependent reactions due to the inflowing gas to take place. Diffusion at the surface results in migration of chemical species to new reactive sites on the substrate whereas reactive-diffusion results in formation of new chemical species which then may desorb back into the reactor chamber.

A comprehensive model thus requires a multi-scale approach; the understanding of all of the elementary atomistic processes occurring at fast time scales, calculation of chemical reaction rates (both gas phase and surface reactions), diffusion processes and thermodynamic data associated with elementary reaction rates. Mesoscale methods are required to model large structures and intermediate time scales.

The proposed research aims to model CVD experiments for CNT synthesis at AFRL with focus on identifying the effects of experimental control parameters and the properties and structures of CNT. A variety of experimental data has shown

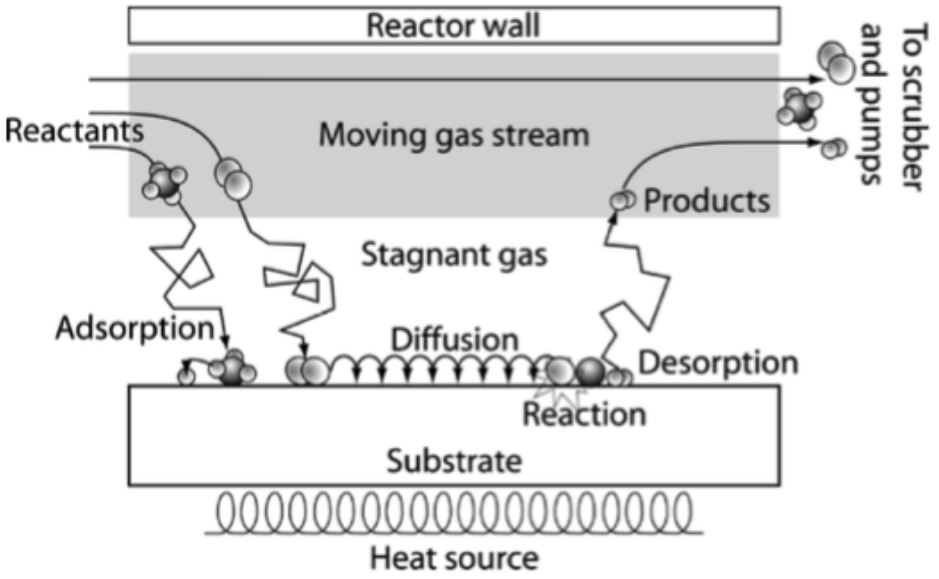

Figure 1.1: A diagram displaying the process of Catalytic Chemical Vapor Deposition using a substrate at an elevated temperature. Involved in the process is a pre-flowed (stagnant) gas and a gas-phase mixture at some particular velocity defined from either turbulent, laminar, or mixed flow regimes. When the carbon precursor flows in with a buffer gas (or a reactive gas) through the stagnant gas a series of chemical reactions will take place. These subsequent products can then form a film on the substrate surface (adsorption). The elevated vibrational energy at the surface of the substrate then allows for the movement of the adsorbed molecules across the surface until bonding occurs which generates products through another chemical reaction (diffusion). Two results can ensue: some products can remain at the surface as non-reactive and form bonds with other adsorbed species or some products can be released (desorbed) from the substrate surface back into the gas-phase. The surface diffusion of solid carbon is a proposed mechanism for CNT cap formation. [1]

a strong correlation between the resultant CNT diameter and catalyst particle size. Other process parameters such as flow rates, carbon precursor, buffer and trace chemical species, temperature distribution, substrate material and design, catalyst metals, etc. also have an effect on CNT synthesis.

1.2 Experimental Approach at AFRL

The purpose of generating a highly involved COMSOL simulation is to capture the physics in a couple of experiments at the Air Force Research Laboratory (AFRL). One reactor is called ARES and incorporates the temperature elevated substrate method

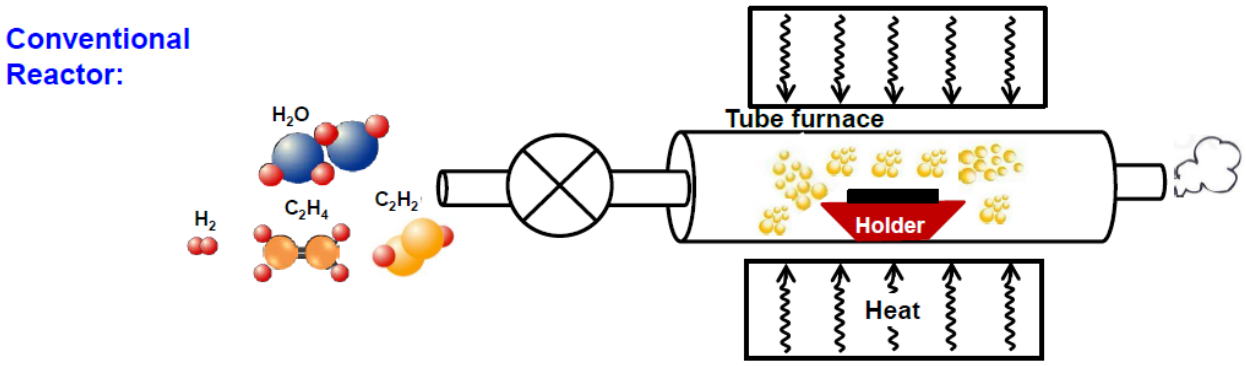

Figure 1.2: Diagram of a conventional CCVD reactor. There is a cylindrical tube through which gases are flowed. The flow can be controlled so that reactions begin in the furnace. The substrate and the cylindrical furnace are held at the same temperature using an ambient heat source.

using a Gaussian laser beam, as can be shown in Figure 1.3. This reactor is similar to ones used in industry, so simulating it is of great importance. The reactor is of a simple cylindrical geometry. The difference being that the substrate is not at an elevated temperature relative to the surrounding gas instead the substrate and the reactor are held at the same temperature through the use of an ambient heat source.

In comparison, Figure 1.2 displays a Chemical Vapor Deposition Reactor, which is the type utilized for the COMSOL simulations in this report. Particular concentrations of ethylene (C_2H_4), molecular hydrogen (H_2), and argon (Ar) are flowed in based off of experimental conditions(where Argon is injected first to remove any air), which constitute the gas mixture. As the gas mixture enters the reactor ethylene begins to dissociate to molecular hydrogen and acetylene. The chemical species undergo a series of chemical reactions until, possibly, amorphous carbon (a-C) is produced. Amorphous carbon is also of interest because it can deposit on the surface of the reactor as well as on the substrate surface resulting in formation of soot. There are various claims that a-C leads to nucleation on the surface to generate initial cap formation. However, the imperfect structure of a-C imparts uncertainty of generating cap formation since CNTs obtained possess a regular lattice structure. Either way, soot formation is very important since any adsorption could reduce the number of surface sites such that carbon could be generated.

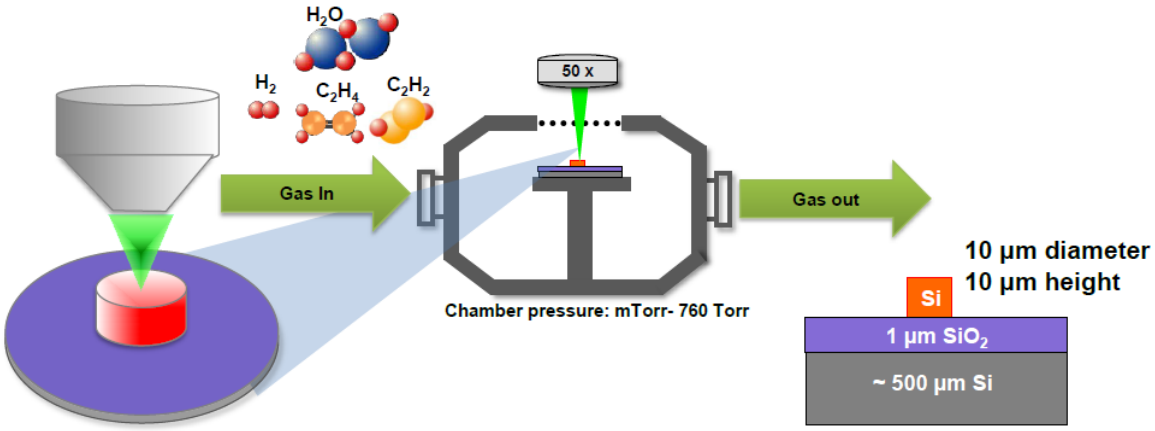

Figure 1.3: Diagram of the ARES (Autonomous Research System) reactor. The make-up of the substrate is shown as well as a diagram of the laser heating and gas flow into the reactor. Raman spectrometry is utilized frequently in order to characterize CNT growth in this reactor. The Raman spectrometers gather the vibrational energy of the system of molecules in order to determine D and G bands which capture defects and characteristic bonding of carbon atoms respectively.

Chapter 2

Technical Approach

This chapter constitutes a general description of the physics involved in a Chemical Vapor Deposition process in a CVD Reactor. Chemical vapor deposition involves the transport of chemically reacting species, mass transport coupled with momentum and energy transfer, and, surface reactions with the substrate in a closed reactor chamber. Computer simulations of continuum mechanics such as reactor geometry, inlet flow rates, thermal boundary conditions, temperature and flow fields, etc. play an important role in the optimization and design of the CVD reactor. The chemical process involved in CVD is captured by a comprehensive chemical kinetics mechanism, transport data, and thermodynamic data for all the chemical species involved in the deposition process.

2.1 Computational Fluid Dynamics

The Navier-Stokes equations are the governing equations for fluid flow modeling along with a particular set of boundary conditions (inlets, outlets, and walls) which describe how the velocity, pressure, temperature, and density of a moving fluid are related. These equations consist of a time-dependent continuity equation for the conservation of mass, momentum conservation,and energy conservation.

In the case of a compressible Newtonian fluid, the momentum equation is:

$$\frac{\partial \mathbf{u}}{\partial t} + \rho(\mathbf{u} \cdot \nabla)\mathbf{u} = \nabla \cdot [-p\mathbf{I} + \mu(\nabla \mathbf{u} + (\nabla \mathbf{u})^T) - \frac{2}{3}\mu(\nabla \cdot \mathbf{u})\mathbf{I}] + \mathbf{F} \qquad (2.1)$$

where ρ is the fluid density, $\mathbf{u}$ is the velocity vector field, and, μ is the fluid dynamic viscosity. The left-hand side term corresponds to the inertial forces and the terms on

the right-hand side describe both pressure forces and viscous forces. The last term is the source term describing external forces applied to the fluid. The above equation is solved together with the continuity equation which describes the relationship between the time rate of change of mass density and the divergence of mass flux.

$$\frac{\partial \rho}{\partial t} + \nabla \cdot (\rho \mathbf{u}) = 0 \tag{2.2}$$

The CFD module in COMSOL is equipped to model most aspects of fluid flow, including descriptions of compressible, non-isothermal, non-Newtonian, two-phase, and porous media flows – all in the laminar and turbulent flow regimes. CFD model parameters used for the current research will be described in relevant sections of this report.

2.2 Chemical Reaction Engineering

The chemical reaction engineering module of COMSOL can be used to solve various reactor types using reaction kinetics, chemical transport and thermal parameters which in turn can be coupled with other modules. When coupled with the CFD module, space-dependent modeling can be performed to account for mass transport, heat transfer, and fluid flow in the CVD reactor using additional modules such as Transport of Diluted Species, Heat Transfer in Fluids, and Laminar Flow interfaces.

Mass transport is an important physical aspect in the simulation of CVD reactor. However, in case of CNT synthesis, CVD reactor modeling of the mass transfer of species occurs together with chemical reactions. This implies that the flux of chemical species is not conserved within a volume element since chemical species may be produced or consumed in such an element. To study mass transfer when there is fluid flow (bulk) along with transport of chemical species in a bath (solute, buffer gas) or to study mass transport of a chemical species in a mixture, a combined convection-diffusion solver must be implemented. The Diffusion-Convection equations are:

$$\nabla \cdot (-D_i \nabla c_i) + \mathbf{u} \cdot \nabla c_i = R_i \tag{2.3}$$

$$\mathbf{N_i} = -D_i \nabla c_i + \mathbf{u} c_i \tag{2.4}$$

where D_i is the diffusion coefficient and in the case of a gas mixture is called the Diffusion Tensor. The variable c_i is the concentration of the i^{th} species, $\mathbf{u}$ is the velocity

field, R_i are the reaction rates for species i , and $\mathbf{N_i}$ describes the mass flux. The LHS terms represent diffusion and convection of the i^{th} species while the RHS term is a source term which corresponds to the species rate expression.

Heat transfer is very important since temperature can affect the density of the gas mixture, which can affect mass transfer, and fluid flow. It can be described through the following equation:

$$\rho C_p \mathbf{u} \cdot \nabla T + \nabla \cdot \mathbf{q} = Q \tag{2.5}$$

$$\mathbf{q} = -k \nabla T \tag{2.6}$$

where ρ is the density of the gas mixture as calculated in the Chemistry Interface in COMSOL, C_p is the specific heat at constant pressure for the gas mixture, T is the temperature of the system, Q are any other heat sources (chemical reaction), k is the thermal conductivity, and $\mathbf{q}$ is the heat flux.

Right away one can see how these equations are analogous to the previous ones. The first term on the left-hand side in the top equation describes the convection of the gas. The density of the gas can change and the velocity field of the gas mixture projected onto the temperature gradient can describe this effect (notice that density directly affects this term). The second term on the left-hand side in the top equation describes the conduction of heat through a material. This can actually be the gas mixture itself and this information can be noticed in the Heat Flux equation. We note that this equation is also assuming steady state for temperature since there is no partial derivative of temperature with respect to time. Lastly, there is a source term, which as stated previously, describes any other heat sources (or sinks) affecting heat transfer. For example, this could be the heat released from an exothermic reaction, or the heat taken from the surrounding due to an endothermic reaction.

Finally, Fluid Flow around the substrate wall is modeled with the Laminar flow interface. The Laminar Flow interface under the Reacting Flow branch combines the functionality of the Single-Phase Flow and the Transport of Concentrated Species interfaces. Mass and momentum transport in a reacting fluid can be modeled from a single physics interface, with the couplings between the velocity field and mixture density set up automatically. This physics interface is applicable to flow in the laminar regime. Inflow at the left boundary is defined in terms of concentration of inlet chemical species. The average flow field is proportional to the pressure difference across the reactor. The CFD module calculates properties intrinsic to fluid flow, such

as: flow patterns, pressure losses, forces on objects subjected to flow, drag and lift, temperature distribution, and variations in fluid composition in a system.

2.3 Chemical Kinetics

A large part of our understanding of the chemistry of the CNT growth process comes from the chemical reactions that occur in the CVD reaction chamber. CFD modeling of CNT growth in conjunction with chemical reaction engineering requires a set of chemical reactions describing all chemical processes in the model, and, transport data and thermodynamic data of all chemical species considered in the chemical mechanism. A reaction mechanism is a compilation of reaction rates for each stage of an overall chemical transformation process. The individual reactions describe consumption or formation for chemical species via a reactive intermediate, activated complex, and/or transitions state. A complete chemical mechanism accounts for all reactants used, the function of a catalyst, stereochemistry, all products formed, and the concentration of each species.

We first consider a simple mechanism for ethylene decomposition into hydrogen and acetylene, in presence of buffer gas M. The reaction can be written as:

$$C_2H_4(+M) <=> C_2H_2 + H_2(+M) \tag{2.7}$$

The "<=>" indicates that the reaction is reversible so that not only does the reactant on the left side decompose but the products react together in order to form the reactant.

The rate constants in the high-pressure limit k_∞ and the low-pressure limit k_0 can written in Arrhenius from as follows:

$$k = AT^b e^{-\frac{E_a}{kT}} \tag{2.8}$$

where A is the frequency factor, E_a is activation energy, k is Boltzmann constant, T and is the temperature at which the rate is computed.

The rate law for the reaction can be written as:

$$r_j = k_j^f \prod_{i=1}^{Q_r} c_i^{-\nu_{ij}} - k_j^r \prod_{i=1}^{Q_p} c_i^{\nu ij} \tag{2.9}$$

This describes the reaction rate for the j^{th} chemical species which is lost due conversion to i^{th} chemical species via the forward reaction $j => i$ and generated via reverse chemical reaction from $j <= i$ reaction in the chemical reaction mechanism. The index i labels the chemical species, Q_r and Q_p are the totals for reactant species and product species respectively, c_i is the concentration of the i^{th} species, ν_{ij} are the stoichiometric coefficients, and k_j^f and k_j^r are the rate constants for the forward($j => i$)and reverse reactions($j <= i$) respectively. The COMSOL software package can import chemical kinetic mechanisms in Chemkin format. Reaction rate parameters for the current project are adopted from various sources and will be explained in the relevant sections of this report.

For pressure dependent reactions (ones containing a (+M) term) a quantity of interest is the third-body efficiency of the buffer gas, which is inert, and acts as a solvent (available in larger quantity) for the reaction. Although the buffer gas does not chemically react, the chemical model becomes more complicated since the rate constant becomes pressure dependent. The pressure dependent rate constant is written in Troe Form as follows:

$$k = \frac{k_\infty}{1 + \frac{k_\infty}{k_0[M]}} F \tag{2.10}$$

where k_∞ is the high pressure limit of the rate constant (concentration of M approaches infinity), k_0 is the low pressure limit of the rate constant (concentration of M approaches zero), $[M]$ is the concentration of the third body, and F is the broadening factor. At higher pressures (or higher concentration of M) the rate constant reaches a constant value, whereas in the low-pressure limit the rate constant equation depends linearly on $[M]$. There is also an intermediate region between where these limits occur called the fall-off region and is described through the use of the broadening factor "F". Just as a note, the Troe Form not containing the broadening factor is called the Lindemann Form, which assumes no need for a correction. The broadening factor (or the correcting term) has the following form:

$$log(F) = \frac{log(F_{center})}{1 + [\frac{log(P_r)+C}{N-0.14(log(P_r)+C)}]^2} \tag{2.11}$$

$$N = 0.75 - 1.27log(F_{center}) \tag{2.12}$$

$$C = -0.4 - 0.67log(F_{center}) \tag{2.13}$$

$$P_r = \frac{k_0[M]}{k_\infty} \tag{2.14}$$

where F_{center} is called the "fall-off parameter" and takes the following form:

$$F_{center} = (1-a)e^{\frac{-T}{b}} + ae^{\frac{-T}{c}} + e^{\frac{-d}{T}} \tag{2.15}$$

where T is the temperature of the system and a, b, c and d are parameters defined for each reaction.

In general, this approach is an approximation based off of empirical results. The Lindemann Form does not correctly capture the fall off region, so through the use of the broadening factor one can approximate the shape of the region transitioning from the low pressure limit to the high pressure limit. The fall-off parameter approximately captures the temperature dependence of a specific reaction, and the dependence on the reduced pressure captures the effect of the third-body. As stated previously, the third-body M can either be one species or a mixture, therefore a generalized form for the concentration of buffer gas, $[M]$, is:

$$[M] = \sum_i \gamma_i [M_i] \tag{2.16}$$

where i represents the i^{th} species in the third-body mixture, the γ_i are the third body efficiencies, and the $[M_i]$ are the concentrations of each constituent species of the third-body mixture. In the case of ethylene decomposition, only one third-body is considered which yields a simple form:

$$[M] = \gamma C \tag{2.17}$$

where C is the concentration of the species. Inserting the above equation into the Troe Form of rate constant yields a generalized way to go from one third-body to another just through changing the given value for the third-body efficiency.

The above formulation is valid only for calculating the forward rate constant. The reverse rate constant needs to be determined in order to complete the formulation. In order to do this, COMSOL automatically generates the equilibrium constant for the reaction through the following equation:

$$K_{eq0,j} = e^{\frac{-H_j}{R_g T}} + \frac{S_j}{R_g} \tag{2.18}$$

where H_j is called the enthalpy of the reaction and is defined by:

$$H_j = \sum_{i=1}^{Q_p} \nu_{ij} h_i - \sum_{i=1}^{Q_r} (-\nu_{ij}) h_i \tag{2.19}$$

where h_i are the enthalpies for each species calculated using a NASA polynomial with coefficients previously defined in a thermodynamic CHEMKIN file.

Further, S_j is the entropy of reaction and is defined by:

$$S_j = \sum_{i=1}^{Q_p} \nu_{ij} s_i - \sum_{i=1}^{Q_r} (-\nu_{ij}) s_i \tag{2.20}$$

where s_i are the entropies for each species calculated using a NASA polynomial.

The equilibrium constant is then used in COMSOL to calculate the reverse rate constant as:

$$k_j^r = \frac{k_j^f}{K_{eq0,j}} \tag{2.21}$$

Finally, thermodynamic properties such as heat capacity, molar enthalpy, and molar entropy of chemical species are described by a set of aforementioned polynomials and are readily available in literature.

Chapter 3

An Adaptation of the CCVD of Gallium Arsenide Example for Ethylene Decomposition

The CVD modeling of a reactor for chemical vapor deposition of GaAs incorporates all major interfaces required for the modeling of CNT synthesis in a CVD reactor. The GaAs model highlights the usability of the Reaction Engineering and Chemistry interfaces together with the Reversible Reaction Group feature for simulation of reaction/transport systems in 0-D and 2D reactor geometry. The Reaction Engineering interface allows for the transient behavior study of different sets of reactions in a perfectly mixed system. The Chemistry interface collects reaction kinetics and calculates transport and thermal parameters, which can seamlessly be coupled with other interfaces. In this model, the Reversible Reaction Group feature is used to import and organize a complex system of bulk and surface reactions that are involved in the CVD process. The space-dependent model accounts for mass transport, heat transfer and fluid flow in the CVD reactor using the Transport of Diluted Species, Heat Transfer in Fluids, and Laminar Flow interfaces. In this chapter, we adapt the GaAs CVD model to and construct CNT growth model.

3.1 0-D Model

As a first step we start with 0-D constant volume batch reactor model to study the chemical decomposition of ethylene. This model does not involve any spatial coordinates, block structures, and meshing which allowed us to focus on the study of

chemical kinetics. GRI-Mech chemical mechanism in Chemkin format (along with transport and thermodynamic data) for C_2 and C_3 hydrocarbon fuel combustion was imported into COMSOL [4]. For the 0-D batch reactor model, the rate of change of concentration of the i^{th} chemical species is written as:

$$\frac{dc_i}{dt} = R_i \tag{3.1}$$

where c_i is the concentration of the i^{th} constituent species and R_i is the reaction rate which has been discussed previously. One could also include Heat balance with the surroundings, but for the time being this was excluded and the reactor was set to a particular temperature (750 K). The reactor volume was set to an arbitrary value, being $1[m^3]$, and various other parameters such as, gas mixture density, pressure using the ideal gas law, activity of each constituent gas was set and the thermodynamic data was imported in the form of NASA polynomials.

The imported C_2-C_3 hydrocarbon GRI-Mech mechanism is very large with hundreds of reactions and thousands of chemical species [4]. To study ethylene decomposition we reduced the mechanism down to two reactions to study the kinetics of ethylene decomposition in an argon (Ar) bath gas. The list of chemical species present in the model is listed in Table 3.1

Species	Concentration($\frac{mol}{m^3}$)
Ar	c_Ar_init
C_2H_2	0
C_2H_3	0
C_2H_4	c_C2H4_init
H	c_H_init
H_2	0

Table 3.1: Table of chemical species considered in 0-D model. The parameters in the right column are predefined in a Global Parameters sections. Note that since Ar is the buffer gas, it is assumed to be in an abundance of concentration. If this concentration was decreased the rate description would alter and, hence, alter the concentration profiles.

The first reaction describes the the decomposition of ethylene to form H_2 and C_2H_2 and the second reaction describes the decompositoin of vinyl radical as described here:

$$C_2H_3(+M) <=> C_2H_2 + H(+M) \tag{3.2}$$

Figure 3.1 shows the concentrations of C_2H_4,C_2H_2 , and C_2H_3 as a function of time. Although there isn't a clear decrease in ethylene concentration, we attribute this to the scale being utilized in Figure 3.1 (logarithmic) and due to magnitude of the rate at the temperature used in our study. The fall in the concentration of ethylene is subtle and is of the order of $10^{-1}[mol/m^3]$.

Further, for testing purposes, the concentration of atomic hydrogen, H, was initialized. Due to its initialization, the production of C_2H_3 is explainable. One mole of each H and C_2H_2 is needed such that C_2H_3 is generated. Also, due to one mole of C_2H_4 required to produce H_2 and C_2H_2, any production of C_2H_2 should be proportional to the production of C_2H_3. One can notice the similar slopes in the C_2H_2 and C_2H_3 plots after a short amount of time, which correlates to the aforementioned intuition. The slopes do not correlate perfectly due to the production of H_2 and the subsequent production of more H and any reversible reactions taken place. In Chapter 4, the analysis of efficiency of reverse production is taken place as a step to develop higher dimensional studies.

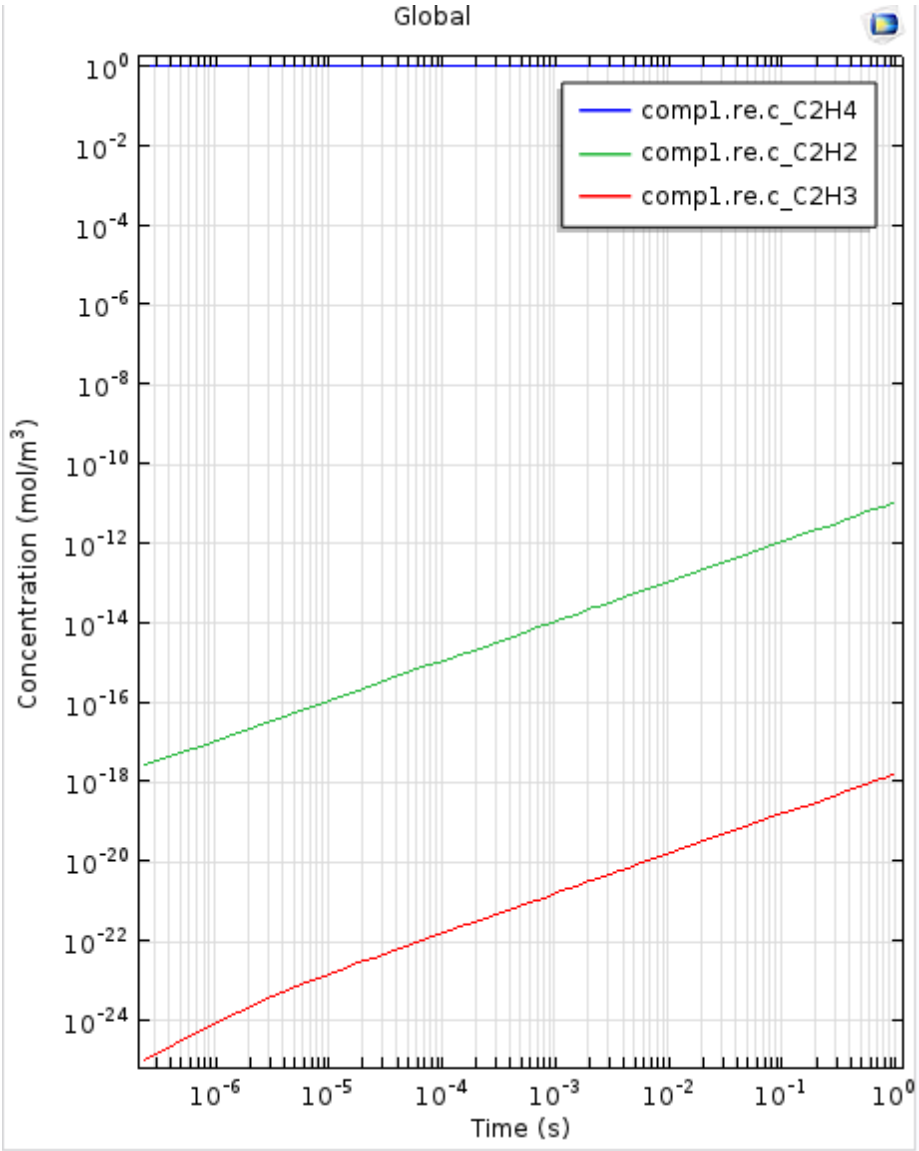

Figure 3.1: Plots of temporal dependent concentrations for C_2H_4, C_2H_2, and C_2H_3

Chapter 4

An Adaptation of the Nitrous Oxide Reduction in a Monolithic Reactor Model for Ethylene Decomposition

In this chapter a description of the NO Reduction in a Monolithic Reactor is presented. The NO Reduction in a Monolithic Reactor simulation is a stationary plug-flow solver (stationary referring to steady state solution for which the molar flow rate is initialized, which directly determines the initial concentration of chemical species. Isothermal and non-isothermal studies is performed to analyze the effect of external heating and reaction rates using different ratios of concentration for nitrous oxide and ammonia is computed to calculate the amount of ammonia released into the atmosphere. A further study of the selectivity, which was a ratio of the two reaction rates, provides information on optimal concentrations with respect to breaking down of nitrous oxide and impede the release of ammonia. The outcome of this study was then applied to a 3-D stationary plug-flow model in a porous geometry (Monolithic Reactor). The NO reduction model was modified to account for the correct chemical reaction mechanism, kinetics, transport, and thermodynamics for CNT synthesis modeling. [3]

4.1 0-D Study of Ethylene Decomposition in a Monolithic Reactor

The preliminary task was to adapt the NO Reduction in a Monolithic Reactor for ethylene decomposition. Using parameter values from GRI-Mech the Troe Form for the rate constants was coded as a local variable in the Reaction Engineering Interface [4]. For the current study, the concentrations of products in the ethylene decomposition reaction was initialized to zero. This is important beacuse the reaction rates and molar flow rates are coupled through an Ordinary Differential Equation which affected the reaction rate analysis.

Since external heating was imperative to the study, an automatic calculation in COMSOL was utilized. The defining equations for the plug-flow reactor including external heating were as follows:

$$\frac{dF_i}{dV} = R_i \tag{4.1}$$

$$c_i = \frac{F_i}{v} \tag{4.2}$$

$$\sum_i F_i C_{p,i} \frac{dT}{dV} = Q + Q_{ext} \tag{4.3}$$

$$Q = \sum_j H_j r_j \tag{4.4}$$

where F_i denoted the molar flow rate of each species, V was the reactor volume, the R_i were the species reaction rates, v was the total volumetric flow rate, the c_i were the species concentrations, T was temperature, C_p was the heat capacity at constant pressure, Q was the external heat, H_j was the enthalpy of the j^{th} reaction calculated from the enthalpy of each species, which were calculated through importing the thermodynamic Chemkin file, and the r_j were the reaction rates for the j^{th} reaction. Further, the external heating, Q_{ext}, was defined using the following relation:

$$Q_{ext} = (T_{amb} - T) * UA \tag{4.5}$$

where T_{amb} was the ambient temperature, T was the temperature of the system calculated by the Reaction Engineering Interface, and UA was the volumetric heat

transfer coefficient. Once this study was set up, plots of reaction rate vs. volume, reaction rate vs. temperature, and temperature vs. volume were generated. Before the plots are displayed it is good to note that the volume had to be defined as a local variable. It was a linear function of time multiplied by $1[\frac{m^3}{s}]$ in order to fix the units. Also, the reaction rate for ethylene was generated using a parametric sweep over the third-body efficiency in order to analyze the effect of different buffer gases. Varying molar flow rates were also used in order to see how this would affect the way the reaction would carry through. The desired reaction temperature was 800 degrees Celsius and when these plots were created, there was a lot of varying in the ambient temperature so the exact value will not be listed although it was normally kept around 700[K] in order to get a good plot range. The plots are shown in Figure 4.1 through Figure 4.4.

We note that in some of the plots there is a minimum negative reaction rate that was reached before becoming positive. It was apparent in Figure 4.2 that the reaction rate only remains negative, but in fact if plotted over a larger range the same anomaly would be noticed. It could also be seen with more reasonable initial values. When an initial concentration is available for both the products and reactants in a reversible reaction, and since the reactions occur at all temperatures (except absolute zero), the reverse reaction occurred briefly which was why there was a dip in the reaction rate plot into the negative range. Negative meant that the reverse reaction is happening, zero meant no reaction is carrying through, and positive meant forward. However, it will be seen that in the 3-D model the molar flow rate of the products can be set to 0 in order to get a more realistic idea of what is happening in the reactor.

Performing the analysis of the direction in which the chemical reaction is taking place (either forward or reverse) is important for higher dimensional studies. Varying the concentrations of the participating species, we were able to determine what would occur (using arbitrary concentrations) if more products in the ethylene decomposition reaction were present initially. Although the rate constant partially defines the reaction rate, the concentration should ideally impede the process taking place to be a pure forward reaction with non-zero values for the products. Plots showed that on a large enough scale for the reaction rate and for the temperature, one will only be able to notice an exponential increase. However, at lower temperatures closer to 800C the reverse reaction rate would always be occurring before the forward reaction. It was shown that the inflection point varies with the concentration–specifically an increase in ethylene. Hence, it could be interpreted that at a low enough production of molecular hydrogen and acetylene, the reverse rate after a particular amount of time will be

unnoticeable. It is also important to point out that experimentally Argon was used as the buffer gas, so altering the ratio of concentration between it and hydrogen would be significant. In fact, this would yield a more efficient ethylene cracking due to a smaller amount of molecular hydrogen being present. This is essentially another way of stating that ethylene will decompose more efficiently than acetylene and hydrogen will combine to form ethylene. In later chapters, we observee that a fairly consistent decrease in ethylene concentration and increase in acetylene is observed using only the ethylene decomposition reaction.

Initial Species	Molar Flow Rate
F_C_2H_4_in	1.5E-4$[\frac{mol}{s}]$
F_H_2_in	1E-4$[\frac{mol}{s}]$
F_C_2H_2_in	1E-7$[\frac{mol}{s}]$
F_AR_in	2.71E-6$[\frac{mol}{s}]$

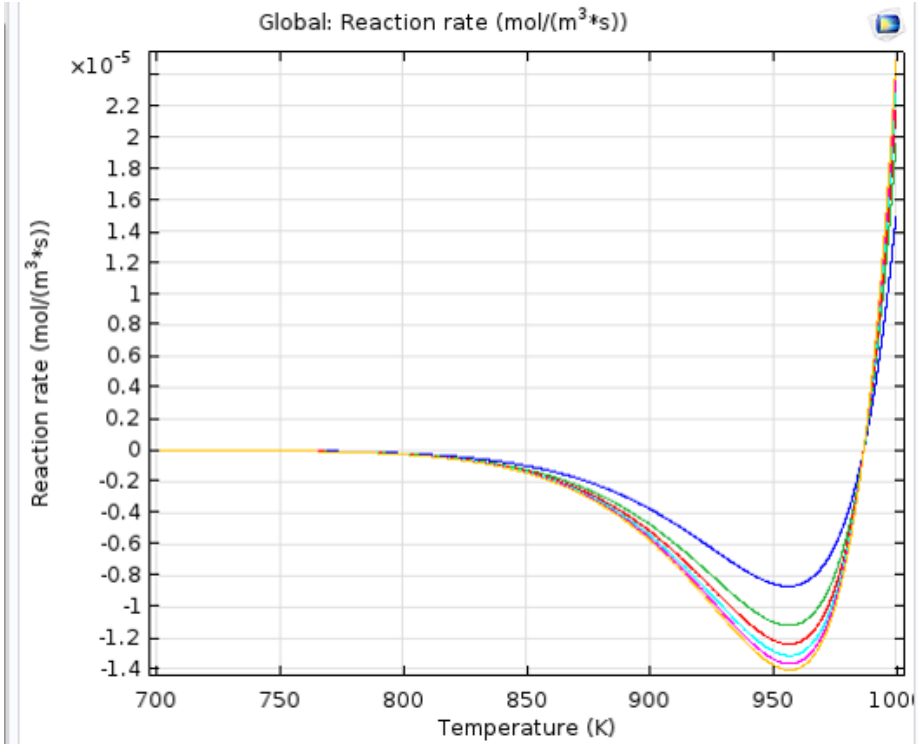

Figure 4.1: Table of molar flow rates of species being analyzed along with a plot of Reaction Rate vs. Temperature using different values for inlet molar flow rates. The difference in each plot is due to a parametric sweep over third-body efficiencies to depict a change in the third-body, but Argon was used as a label since it is going to be used later.

Initial Species	Molar Flow Rate
F_C_2H_4_in	1.5E-3$[\frac{mol}{s}]$
F_H_2_in	1E-4$[\frac{mol}{s}]$
F_C_2H_2_in	1E-7$[\frac{mol}{s}]$
F_AR_in	2.71E-6$[\frac{mol}{s}]$

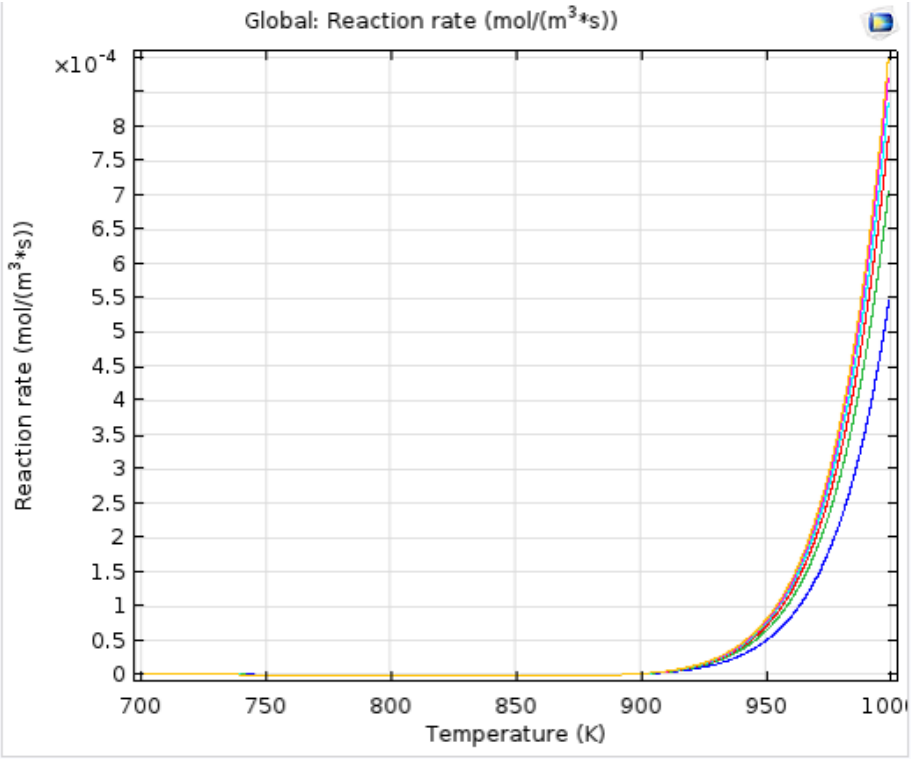

Figure 4.2: Reaction Rate vs. Temperature after changing the initial molar flow rate of ethylene to a value 10 times larger compared to the first study.

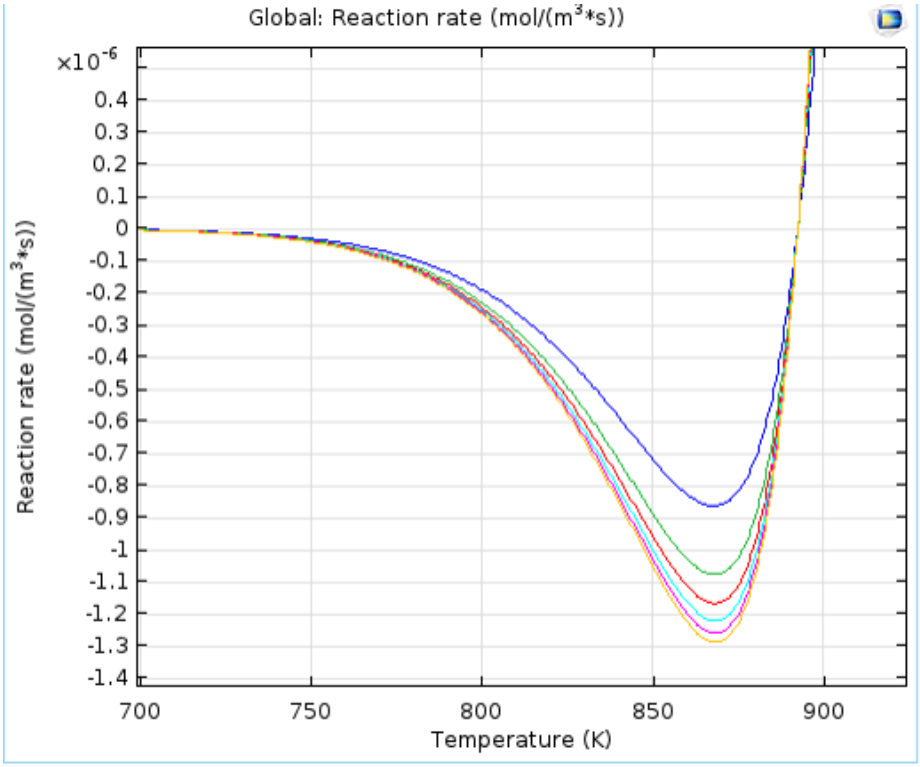

Figure 4.3: This is the same plot as in Figure 4.2 but zoomed in

Initial Species	Molar Flow Rate
F_C_2H_4_in	1.5E-4$[\frac{mol}{s}]$
F_H_2_in	1E-4$[\frac{mol}{s}]$
F_C_2H_2_in	1E-6$[\frac{mol}{s}]$
F_AR_in	2.71E-6$[\frac{mol}{s}]$

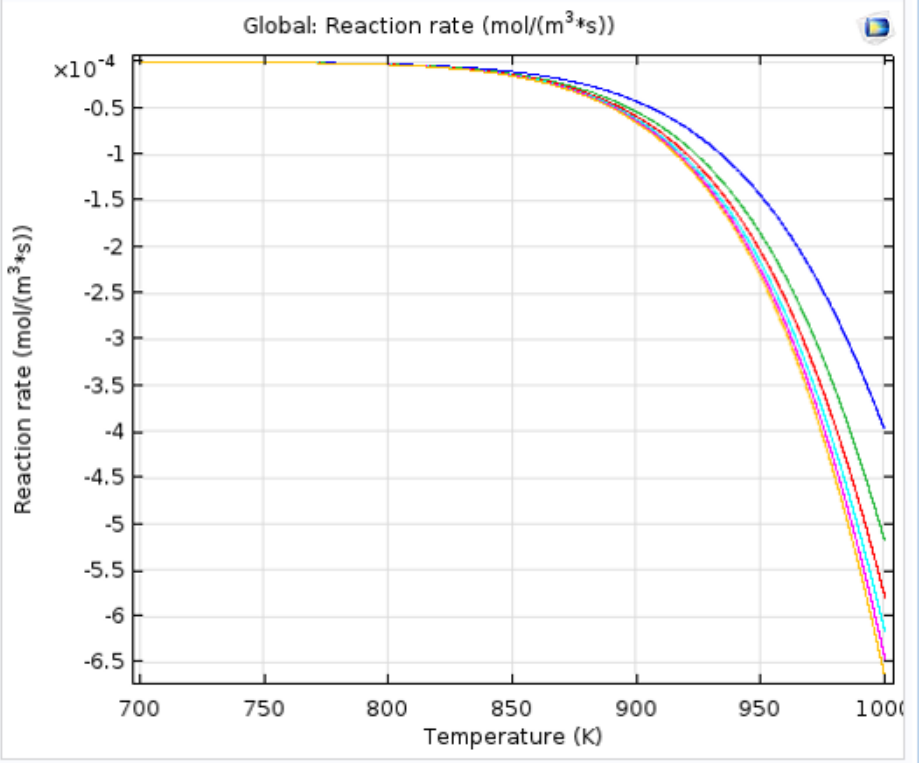

Figure 4.4: Reaction Rate vs Temperature after altering the initial molar flow rate of acetylene to a value 10 times larger compared to the first study.

Chapter 5

3-D Model of Ethylene Decomposition in a Monolithic Reactor

Starting with the 3-D model used in the NO Reduction in a Monolithic Reactor model was useful due to the aforementioned point that the chemical reaction mechanism was a lot smaller in comparison to the GaAs example and the physics was a lot simpler. Hence, incorporating a single reaction was not a problem. COMSOL was useful because it allowed the ability to automatically generate a higher dimensional model after starting a 0-D study. More focus was invested on the 3-D model since these were the results that will be more relevant. Right away, based off of the 0-D model, a lot of attention was focused on defining the molar flow rates. Molar Flow rates defined "how much" of a substance flowed per unit time with units of moles per second. It could actually be calculated using the ideal gas law, which was an assumption that can be made for the time being, using the following relation:

$$F = \frac{dn}{dt} = (\frac{P}{RT})(\frac{dV}{dt}) \tag{5.1}$$

which was just a time derivative of the amount of moles. Since pressure, the ideal gas constant, and temperature can be assumed as constant the only other relevant time derivative was that for the volume, V. The time derivative of volume yielded what was called the volumetric flow rate. This happened to be measured in units of SCCM, which could be converted to SI units. Further, the 3-D model being utilized meant that a numerical mesh had to be generated in order to perform the computations of

interest. This more elaborate process allowed for the initialization of the molar flow rate of the products to 0.

The chemistry involved with this model was not difficult to incorporate since it was imported from the 0-D model. The only difference was that it did not make sense to perform a parametric sweep in a 3-D environment, so a third-body had to be defined. Since argon was the most commonly used it was chosen. It had to be checked that the molar masses were imported correctly so that variables imported into other interfaces wouldn't compute errors, such as calculating the Diffusion Tensor.

The Mass Transport was fairly straightforward as well since the geometry and fluid flow interfaces hadn't been changed right away. A porous medium defined as constituent, wall-separated reaction channels filling the volume was being used, which meant it was apparent that no mass flow would occur between constituent reactor channels. This allowed the Diffusion Tensor to be simplified. It contained only one component, for each species, along the reactor channel's axis. Further, the more easily manipulated molar flow rates could be used as initial values in the model. Various boundary conditions had to be employed such as: the previously mentioned initial concentrations, no diffusion normal to the outlet, no mass flux on the reactor's outer surface and internal supporting walls, and the incorporation of the velocity field calculated from Darcy's Law in the domain. These were fairly simple for the most part since importing the velocity field was an automatic selection supported by COMSOL and the mass flux conditions were set by default.

The Heat Transfer Interface, on the other hand, was one of the more difficult interfaces to implement. In the original model, the nitrogen molecule was defined as a material with properties that were predefined as well as an arbitrary material for the interior supporting walls. These were created in order to define both heat transfer in solids and liquid domain conditions. The transfer through the solid supporting walls made a lot of sense since all of the properties (thermal conductivity, density, etc.) were linked in from the interface where the materials were defined. However, there were problems with trying to make sense of the heat transfer in liquid conditions. COMSOL arbitrarily defined a thermal conductivity matrix and pulled in the other aforementioned values from the material. It made more sense that the heat transfer in fluids interface should be defined entirely from the gas mixture. COMSOL automatically calculated thermal conductivity and density for the gas mixture in the chemistry interface and could be selected to be linked in to the heat transfer interface. Further, there were issues with how the temperature throughout the reactor and at the inlets should be defined. Initially, it made sense to keep the inlet at room

temperature and the reactor channel domains (space constrained by boundaries of the constituent reactor channels) at 800 degree Celsius, but then the concentration wouldn't be computed in a reasonable way, i.e. there were stripes on the reactor surface instead of a change happening inside the channels. This outcome can be noticed in Figure 5.1. So, after thinking about the reactor setup it seemed more reasonable to have the inlet, outlet, and domain initially at the same temperature (800 degrees celsius or 1073.15 kelvin equivalently) since one could think of the reaction happening inside an enclosed volume. This greatly affected the concentration and temperature distributions which can be seen in Figure 5.2. Further, the NO Reduction model assumed that heat could escape to the environment through the reactor surface and dissipate through the interior supporting walls. In the study of interest, there had to be a consideration that there was insulation and there would be no heat flux through the reactor surface. This greatly simplified the solution.

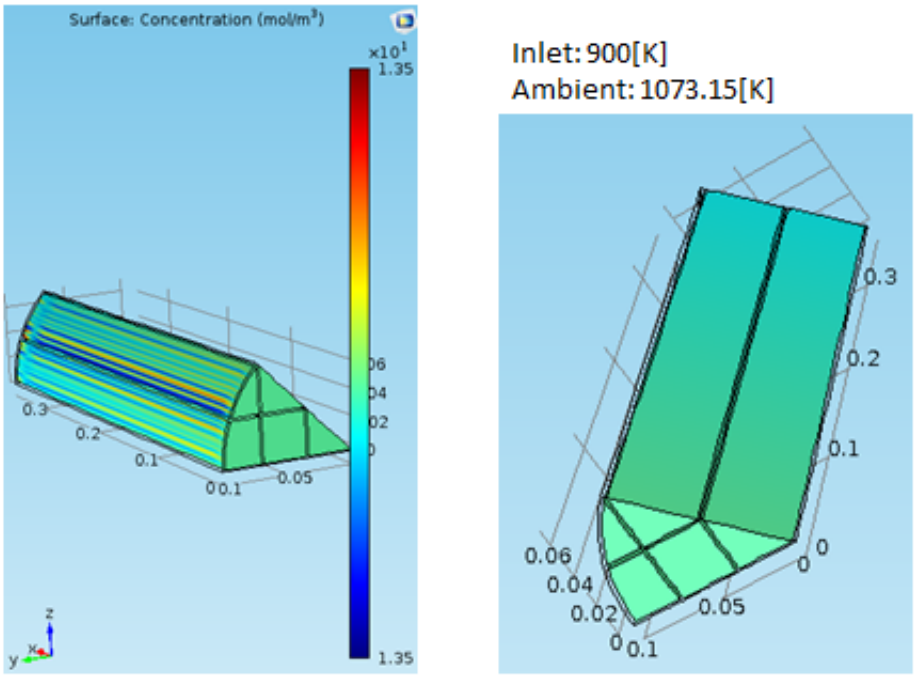

Figure 5.1: A concentration plot with an inlet temperature quite a bit higher than room temperature, but the effect was the same. The concentration stayed fairly constant throughout the reactor channel domains and most of the change was occurring at the reactor channel surface showing up as stripes. Note that at this point Darcy's Law was still being implemented and changes to Heat Transfer in Fluids had not taken place.

As was previously stated, since the geometry being utilized was a porous medium Darcy's Law could be used. However, after completing a computation of the Reynold's

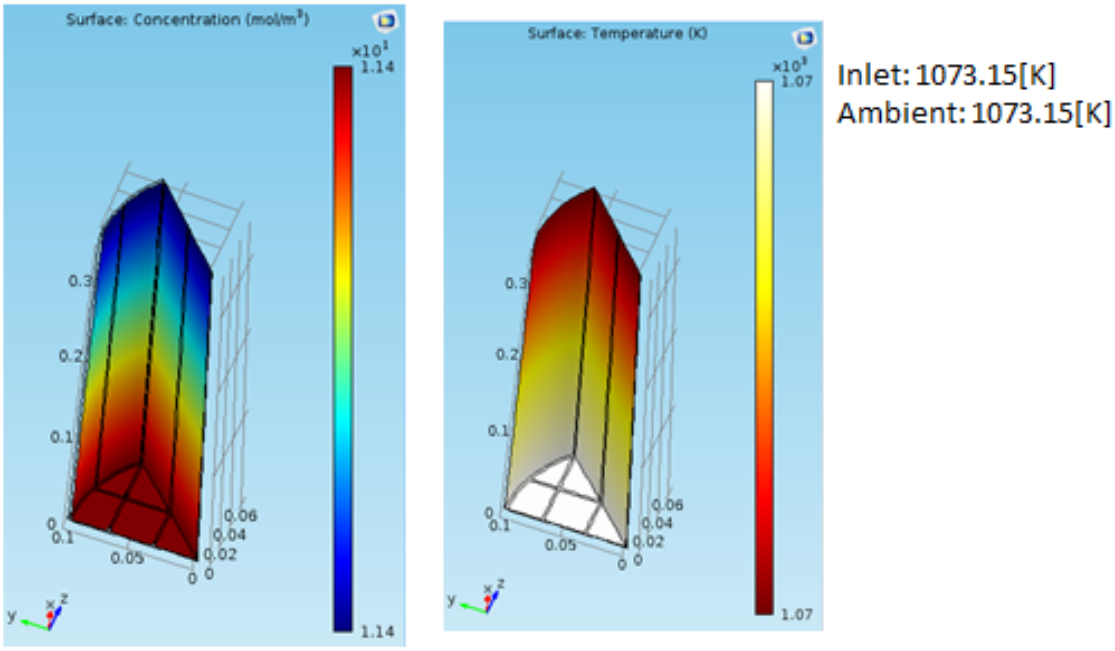

Figure 5.2: Concentration of ethylene and temperature distribution throughout the reactor channels using the same Inlet and Ambient Temperatures and initial temperature throughout the channels. This was a lot more realistic. It is important to note here that the Heat Transfer is occurring through Argon being treated as a liquid. The change to using material properties has not occurred. It is important to note that the outlet temperature has not been set to be the same as the inlet and ambient temperatures. Also, Darcy's Law is still in place.

Number for the experimental reactor of interest along with the current conditions allowed for Laminar Flow, the Reynold's Number was calculated to be around 17.6 which was extremely low. This could be understood since the reactor diameter was very small (46 mm) and exceptionally low values for the volumetric flow rates (600 SCCM in total) were utilized. Hence, it had to be kept in mind that there would be an inevitable change occurring from Darcy's Law to Laminar Flow. The fluid flow needed to be studied in a lot more detail, since Laminar Flow is indeed complicated, but a lot has been gathered from the study using Darcy's Law. With Darcy's Law, the mass flux was assumed to be constant and the velocity field was assumed to originate from a pressure gradient. Also, when defining the boundary conditions it was assumed that the inlet and outlet velocities would not be the same. This was another change that had to occur. Further, there were difficulties with understanding the pressure. When defining the boundary conditions, an initial pressure must be defined at the inlet, outlet, and reactor domain. This happened to be the pressure

of the system as calculated as an independent variable in the Fluid Flow Interfaces. However, there was an absolute pressure which was the sum of the reference pressure and the aforementioned pressure variable. Absolute pressure was what COMSOL used when calculating overall pressure because it took the atmospheric conditions into consideration–the reference pressure was set at 1[atm] in order to take care of these atmospheric considerations. Hence, it ended up not being too complicated to transfer over the fluid flow interface to Laminar Flow since many things would remain the same, except that there weren't as many assumptions when simplifying the Navier-Stokes Equations.

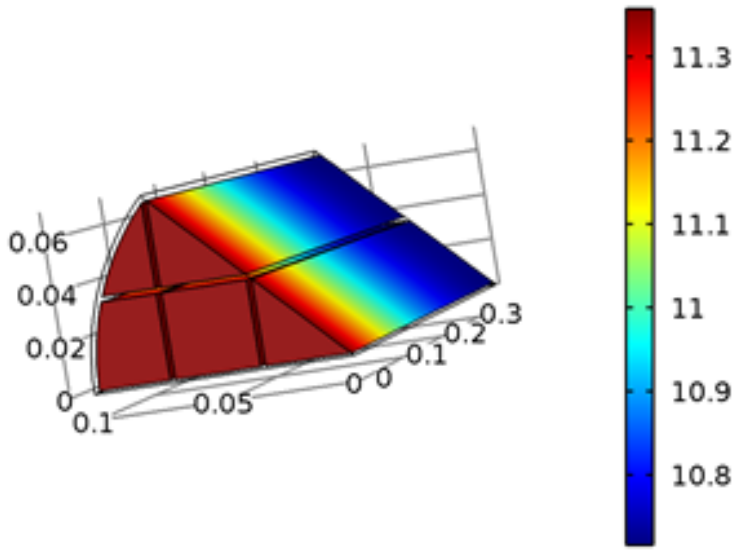

Figure 5.3: Concentration of ethylene after changing the thermal conductivity and including Laminar Flow in the model.

Since the physics seemed to be setup the way that was desired, the most logical route to take was to define a new geometry that would be more similar to the one that needs to be modeled. Before getting to that, it must be noted that there were a few issues getting Laminar Flow to work correctly. The most notable being that in this model the initial velocity was set as a zero vector and the inlet velocity had to be set as a vector along the direction of the reactor channels (which is the same as having a normal velocity) but the outlet velocity could be set to a normal one without using a vector. It was taken care of and utilized in the new geometry model.

The newly generated geometry was a cylinder with dimensions (46mm diameter and 1m length). The heat transfer through solids could be ignored since the interior

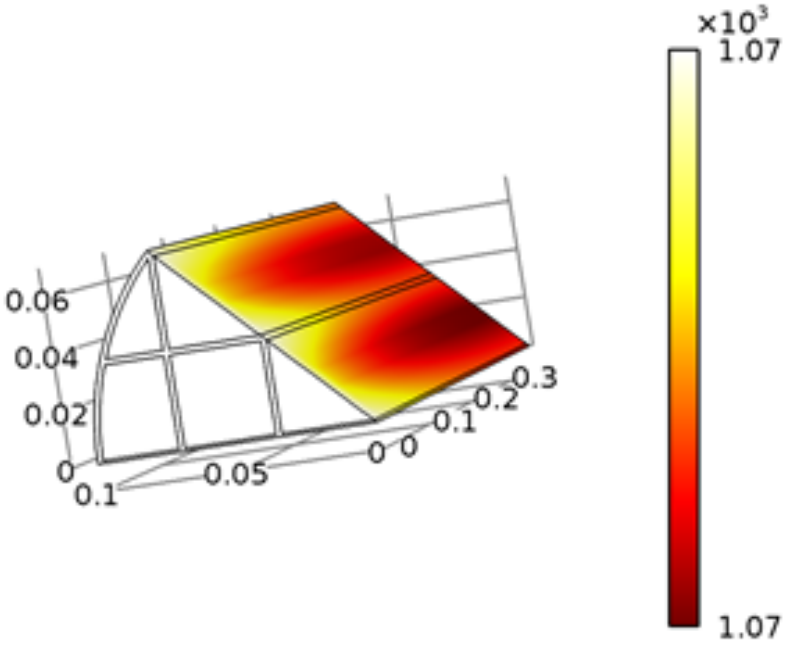

Figure 5.4: Temperature distribution in the reactor channels after changing the thermal conductivity and including Laminar Flow without setting the inlet and outlet temperatures to be the same yet.

supporting walls were removed and there were fewer domains and boundaries to consider. The output using the new geometry was included in Figures 5.5 and 5.6.

As one can notice in Figure 5.5, along the reactor centerline, the concentration of ethylene decreases from the inlet at 0[m] to the outlet at 1[m]. This outcome aligns with the prediction using the 0-D analysis. The solutions generated were at steady-state through the use of the BDF numerical solver, which will be discussed later.

Further, since it was determined that the forward reaction within the ethylene decomposition reaction would dominate, one should also notice a decrease in reactor temperature since the reaction is indeed endothermic. As was discussed earlier, for the purpose of this study, the inlet, outlet, reactor surface, and domain were all set to 800C. This explains why temperature does not decrease significantly at the inlet and outlet–the bulk of the decomposition takes place toward the center of the chamber.

Although fluid flow is imperative to the analysis, the results from Laminar Flow were not yet included because the 2-D cross-section in figure 6.7 was essentially the same, aside from the profile near the substrate's surface. Due to the lack of internal geometry (substrate), the velocity profile is intuitive. Since there is a no-slip condition at the surface, it was observed that the velocity was a maximum at the reactor centerline and decreases toward the surface radially. Due to the expansion of the gas,

there is a slightly different characteristic near the inlet and outlet. Once again, this will be discussed more thoroughly in the next chapter.

The main purpose of this study was to develop an intuitive basis such that a time-dependent analysis could be generated. However, in order for deposition to occur a substrate had to be included in the geometry. The figures in this chapter are not transparent, and hence, do not display exactly what is occurring within the reactor domain. Due to the symmetry of the cylinder, the geometry could be condensed to 2 dimensions without any loss of generality. This approach led to more efficient convergence and will be discusses in Chapter 6.

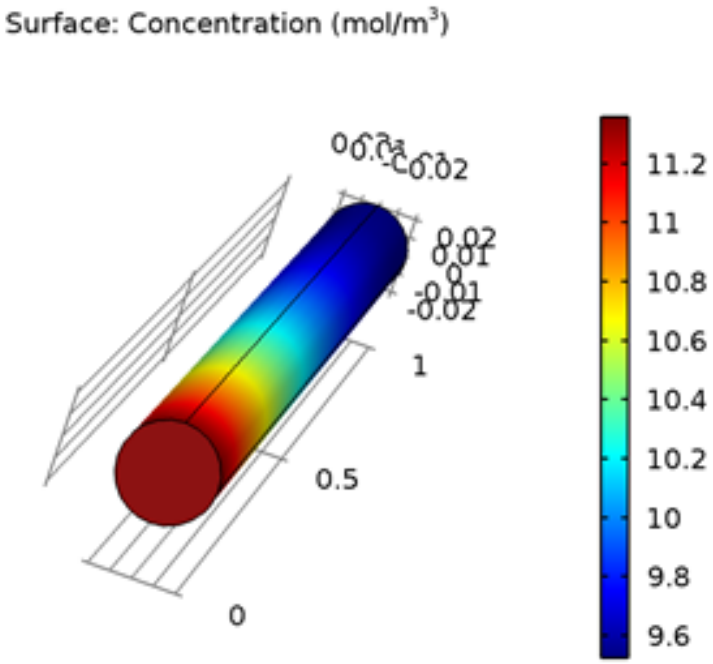

Figure 5.5: The concentration of ethylene throughout the reactor channel. Note that the inlet starts at the point 0 along the reactor channel going up to 1 meter. This outcome makes sense since Ethylene Decomposition dominates over the reverse reaction at high enough temperatures as was seen in the 0-D model.

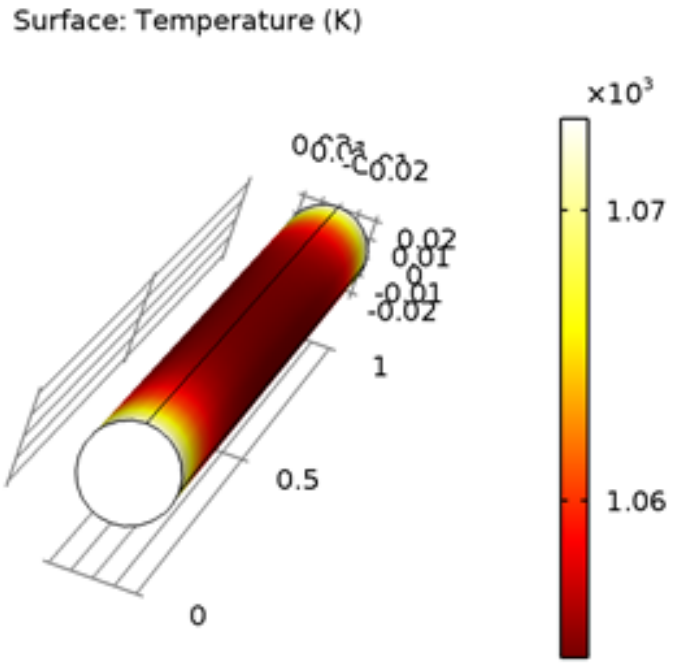

Figure 5.6: Temperature distribution throughout the reactor after setting the inlet, outlet, and initial domain temperatures to be the same. This makes sense since ethylene decomposition dominates and is an endothermic reaction which means heat will drop away from the inlet and outlet.

Chapter 6

Modeling of a Chemical Vapour Deposition Reactor in 3-D

This chapter will cover the development of a 3-D, time-dependent study in the cylindrical reactor of interest. A complete gas-phase and surface reaction list will be generated for future use. Specifically, a gas-phase reaction mechanism was incrementally incorporated to analyze amorphous carbon development which will be observed in later chapters.

6.1 Reactor Geometry

The present study focuses on importing a reduced chemical mechanism for ethylene decomposition and the study of gas-flow patterns in a 3-D CVD reactor with a substrate for CNT growth.

The CVD reactor is modeled as a cylinder with 1m in length and 46mm in diameter. The substrate is defined to have a rotation of -30 degrees with dimensions of width equal to 0.008m, a height of 0.03m, and a depth of 0.008m. The 2D cross-section of the reactor is shown in Figure 6.1. A time-dependent simulation is implemented in order to study the thermal decomposition of the gas-phase molecular species and to calculate the concentration of molecular species throughout the reactor domain and around the substrate surfaces. A complete physics model includes the coupling of Heat Transfer in Fluids, Mass Transport of Diluted Species, Laminar Flow, and Chemical Reaction Engineering modules of COMSOL.

Figure 6.1: Cross-sectional view of the CVD reactor with the substrate at a distance of 0.5 m from the left boundary which is defined to be the inlet port. The substrate is defined to have a rotation of -30 degrees with the dimensions of a width 0.008m, height of 0.03m, and depth of 0.008m.

6.2 Mass Transport of Diluted Species

The Chemistry interface of COMSOL is used to import chemical mechanisms, thermodynamics data and transport data in Chemkin format. A parameter that is frequently used in heat-transfer calculations is the thermal diffusivity, The thermal diffusivity α is described by the following equation:

$$\alpha = \frac{k}{\rho c_p} \tag{6.1}$$

where k is the thermal conductivity, ρ is density and c_p is heat capacity. Thermal diffusivity is set in the chemistry interface and these are then imported into the Mass Transport module (as was done in the stationary solution) in order to include the source terms on the right side of the diffusion equation and the computed diffusion coefficients appear on the LHS of the diffusion equation. The diffusion coefficients are isotropic and defined from the aforementioned diffusivities. To define boundary conditions at the solid interface, so that no diffusion would occur through the solid substrate, material properties were imposed along with no mass flux conditions on the surface.

The initial concentration of species throughout the reactor domain also had to be set, not including the substrate since it has already been defined as a solid allowing no mass flux. As will be discussed in the Section 3, concentrations only of species of interest are not initialized to zero since most of the gases will not be present in the

domain in the initial state (In fact only H_2 will be initialized). However, at the inlet there must be a defined concentration for any inflowing gas which was not initially introduced to the domain. Since the solvent is remaining at a constant concentration its conditions do not have to be set explicitly as discussed previously.

For the case of CVD it is common that mass and heat convection will be a dominating source of energy transfer, so the definitions in the mass transport interface of COMSOL allow the input of "convection" as a transport mechanism which means that diffusion normal to the outlet is set to zero. The diffusion term is defined in the Mass Transport equation in equation (2.3).

6.3 Heat Transfer in Fluids

Similar to the case for the mass transfer interface, properties of the gas mixture can easily be incorporated into the heat transfer module. These were utilized in the stationary results as well, but have been altered due to further reactions being included. In order to incorporate the substrate into this interface, the aforementioned material properties as defined from the stationary solution in the "NO Reduction in Monolithic Reactor example" had to be included so as to capture thermal conductivity, heat capacity, and density [3]. Initial temperatures were set at 1073.15 [K], as was done previously, at the inlet and throughout the domain of the reactor. However, since material properties were included for the substrate no temperature was initialized at the boundary nor through the domain of the substrate. As was also stated, the source terms were set to heat sources from the reaction, which happen to be endothermic, in the heat transfer equation. In order to complete the boundary conditions for heat transfer, the outlet condition was changed from including the same initial temperature to including the aforementioned condition which states that there is no heat flux through the outlet. Hence, energy transfer at the outlet is dominated through the convection in the gas of CVD.

6.4 Laminar Flow

Alterations in the Laminar Flow interface began with the definition of compressible flow. Previously, it was simply assumed that the flow is compressible since it is a gas (without considering Mach Number calculations) which automatically places the Mach Number less than 0.3. Since (referring to COMSOL's page on compressible flow) the Mach Number is defined as the ratio of the magnitude of the average gas-

phase velocity and the speed of sound, the Mach Number will be much less than 1 given the volumetric flowrates discussed previously. This means that the flow is indeed incompressible, similar to a liquid.

Many of the boundary conditions for Laminar Flow are similar to the set up for the stationary study, except that no slip conditions had to be imposed on the substrate surface. As a reiteration of the conditions included, fluid properties such as density and dynamic viscosity have been brought in from the chemistry interface, velocity and gauge pressure has been initialized to zero throughout the domain, a normal inflow velocity was defined at the inlet, and a zero gauge pressure with suppressed backflow at the outlet.

6.5 First Time-Dependent Study

In a similar way to the stationary solution, concentration plots were generated for each gas species. To perform further analysis, two more reactions were included in the study:

$$C_2H_2 + H + Ar <=> C_2H_3 + Ar \tag{6.2}$$

$$H_2 + Ar <=> 2H + Ar \tag{6.3}$$

As a reminder, ethylene decomposition is described by the following reaction:

$$C_2H_4(+M) <=> C_2H_2 + H_2(+M) \tag{6.4}$$

where M is the third-body, either as a gas mixture or an inert buffer gas, being Ar in our case.

The output for a time-dependent study is a set of plots at time intervals defined in the study settings within COMSOL's Application Builder. The time range utilized was 0 to 200 seconds at 20 second intervals. Since H_2 is flowed into the reaction chamber before other gases, the initial concentration within the domain is set to be the same as the inlet concentration. As a reminder, the flow rates for inflowing species are: 470 for Ar, 100 for H_2, and 30 for C_2H_4 in units of SCCM (Standard Cubic Centimeter per Minute). The concentrations are defined from the ratio of the molar flow rate (defined from the ideal gas law) with the total volumetric flow rate. Since the definition of the fluid flow is the same as for the stationary solutions, the normal

inflow velocity remains the sum of the volumetric flow rates of initial species divided by the cross-sectional area of the reactor (diameter at 46mm). However, in the previous study H_2 was incorrectly excluded from the sum as has been incorporated in order to create more accurate results.

As was discussed previously, since the substrate has been included in the study, material properties have been used in order to accurately define heat transfer. These solid properties have been carried over from the "NO Reduction in Monolithic Reactor" example when the "walls" were defined [3]. The values for the density, heat capacity at constant pressure, and thermal conductivity are shown in Figure 6.2.

Figure 6.3 shows the concentration of ethylene at various times in the CVD reac-

Density	Heat Capacity at Constant Pressure	Thermal Conductivity
$2970[\frac{kg}{m^3}]$	$975[\frac{J}{kg*K}]$	$35[\frac{w}{m*K}]$

Table 6.1: Substrate Material Properties

tor chamber. At time $t = 0$ ethylene is injected into the reaction chamber and gas flow carries molecular mass towards the outlet. Ethylene undergoes thermal decomposition as described by Reaction (6.4) and, therefore, we observe a smaller concentration of ethylene gas in the reaction chamber. However, ethylene consumption is slightly countered by the constant replenishment due to the C2H4-Ar mixture.

Figure 6.4 shows the concentration of acetylene as a function of time and space in the CVD reactor. Acetylene is formed due to the thermal decomposition of ethylene and, at the initial time, we observe a higher concentration of acetylene on the inlet-side of the substrate compared to the outlet-side. It is also shown that the concentration of acetylene reaches a steady state value at longer times. Since the flow rate of ethylene is held at a constant, the mole balance on acetylene species in a differential segment of the reactor volume is directly proportional to the reaction rate of Reaction (6.4) and since the volume of the plug is chosen to be sufficiently small there is no variation in reaction rate within this volume. Hence, the concentration of acetylene per unit volume is expected to reach a steady state value as governed by the reaction rate. The concentration of acetylene further depends on the reaction and diffusion of dilute species in the gas mixture.

Hydrogenation of acetylene leads to the formation of the vinyl-radical (C_2H_3) as described by Reaction (6.2). Figure 6.5 shows the concentration of the vinyl-radical in the reactor volume at various times. We observe that the concentration of acetylene is much smaller compared to the concentration of ethylene and furthermore, due to the

lower concentration of acetylene, the concentration of the vinyl-radical in the CVD reactor is orders of magnitude smaller compared to both the ethylene and acetylene molar concentrations. Since the vinyl-radical is formed by addition of hydrogen to acetylene, the concentration of acetylene also depends on the concentration of the H atom (shown in Figure 6.4), which in-turn, depends on the concentration of H_2 in the CVD reactor and the thermal decomposition rate of H_2 as described by Reaction (6.3).

The concentration of H_2 is not shown since it does not change significantly over the time range utilized.

Figure 6.6, shows the concentration of H atoms in the CVD reactor chamber as function of time. H atoms only appear as the product of reaction (6.3) which is the thermal decomposition of H_2, and, are consumed by the hydrogen addition reaction of acetylene, reaction (6.2).

The temperature plots shown in Figure 6.7 also make it apparent that the forward reactions are dominating throughout the process due to the decrease of approximately $10K$. This is attributed to the fact that each reaction displayed is endothermic overall, which is causing the decrease in temperature. It may be predicted that a gas-mixture should have a higher thermal conductivity, however, based off of the results it seems as if the conductivity is lower since the temperature isn't remaining homogeneous. It is also important to note that the thermal conductivity appears to be higher than the solid since over the 0 to 200s time range the substrate temperature doesn't drop significantly. As stated, the value for this thermal conductivity is tentative and may show different results once changed. The gas-mixture thermal conductivity will also be checked for accuracy as well.

Finally, the gas-phase velocity plot shown in Figure 6.8 clearly displays the Laminar Flow taking place. Since the boundary conditions were set so there is no slip at the reactor surface and the substrate surface, the velocities are zero at these locations. Note that there is a velocity gradient from the surface to the center where it is highest (comparable to the initial velocity) due to the inertial forces causing the gas-mixture to slow from the boundary conditions.

The Laminar Flow interface also generates the Gauge Pressure plot which is shown in Figure 6.9. The accuracy of the pressure gradient must be checked as well, but qualitatively it is reasonable since the zero-pressure outlet condition is present and this pressure drop shows the pressure build-up from gases flowing in at the inlet. Since the gas is flowing in and out this pressure does not change.

Although aspects of the results are reasonable, there are a few observations which

do not match up with intuition. In particular, which will be shown in a later stationary study, when velocity is varied the concentration of participating species within the ethylene decomposition reaction will also vary. Specifically, with a decreased concentration (or increased residence time in the reactor) the cracking of ethylene becomes more efficient. On another note, if the temperature is increased the cracking would become more efficient (which is also observed in later studies). This also implies an effect on the velocity. If the temperature is relatively larger within the reactor, then the pressure should be increased which would also increase the velocity.

One expects, due to the decreased cross-sectional area, an increased velocity which would align with the previously discussed intuition. However, given the results intuition is not captured. This is fine since the purpose of this study was to not necessarily obtain perfect results, but to generate a template for optimization. Since 3-D is complicated, and given the symmetry of the reactor geometry being utilized, a 2-D time-dependent study was directly developed from the 3-D model in order to simplify and attempt to correct any inconsistencies being observed.

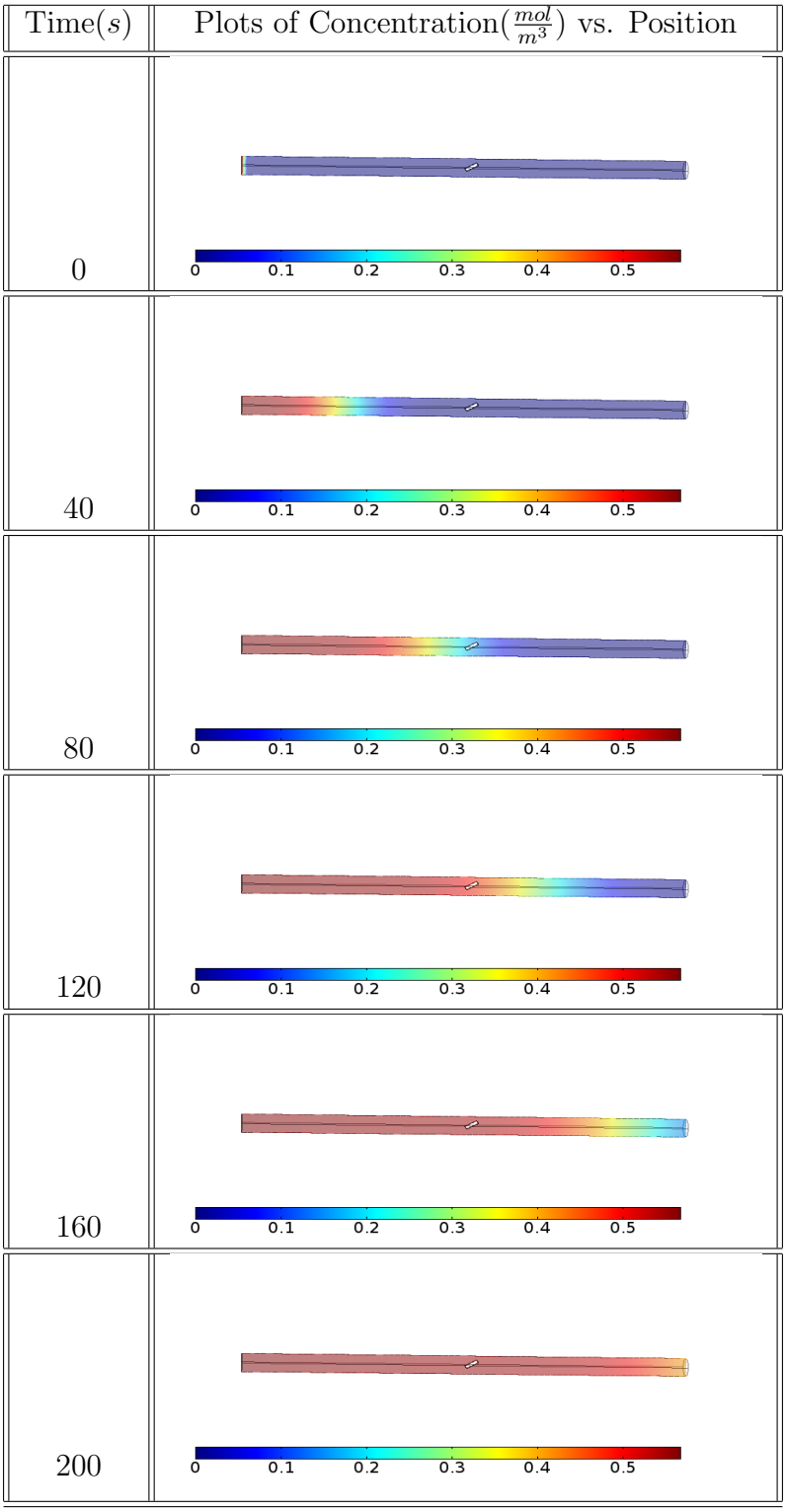

Figure 6.2: C_2H_4 concentration from 0 to 200s at 40 second time intervals.

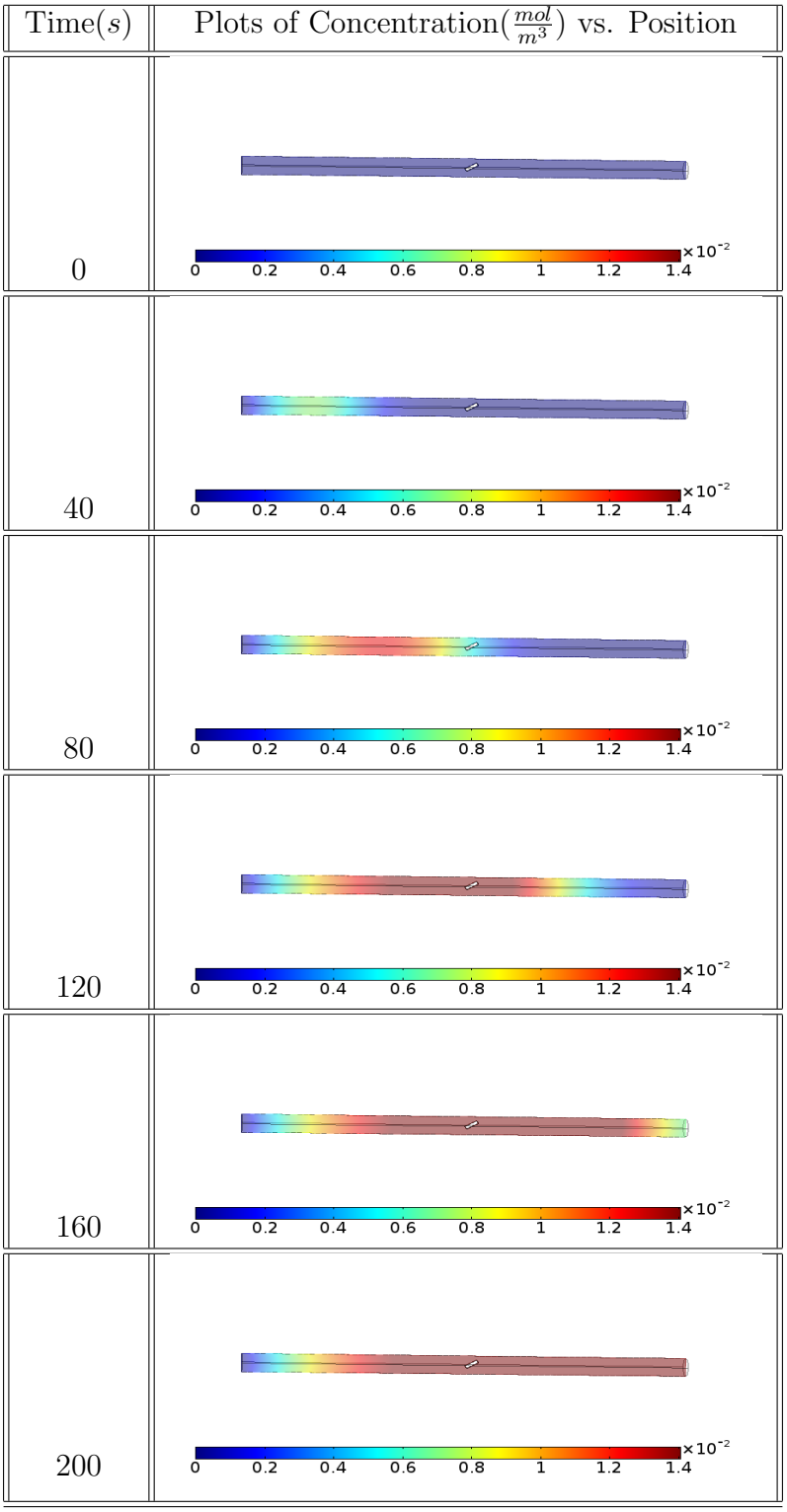

Figure 6.3: C_2H_2 concentration from 0 to 200s at 40 second time intervals.

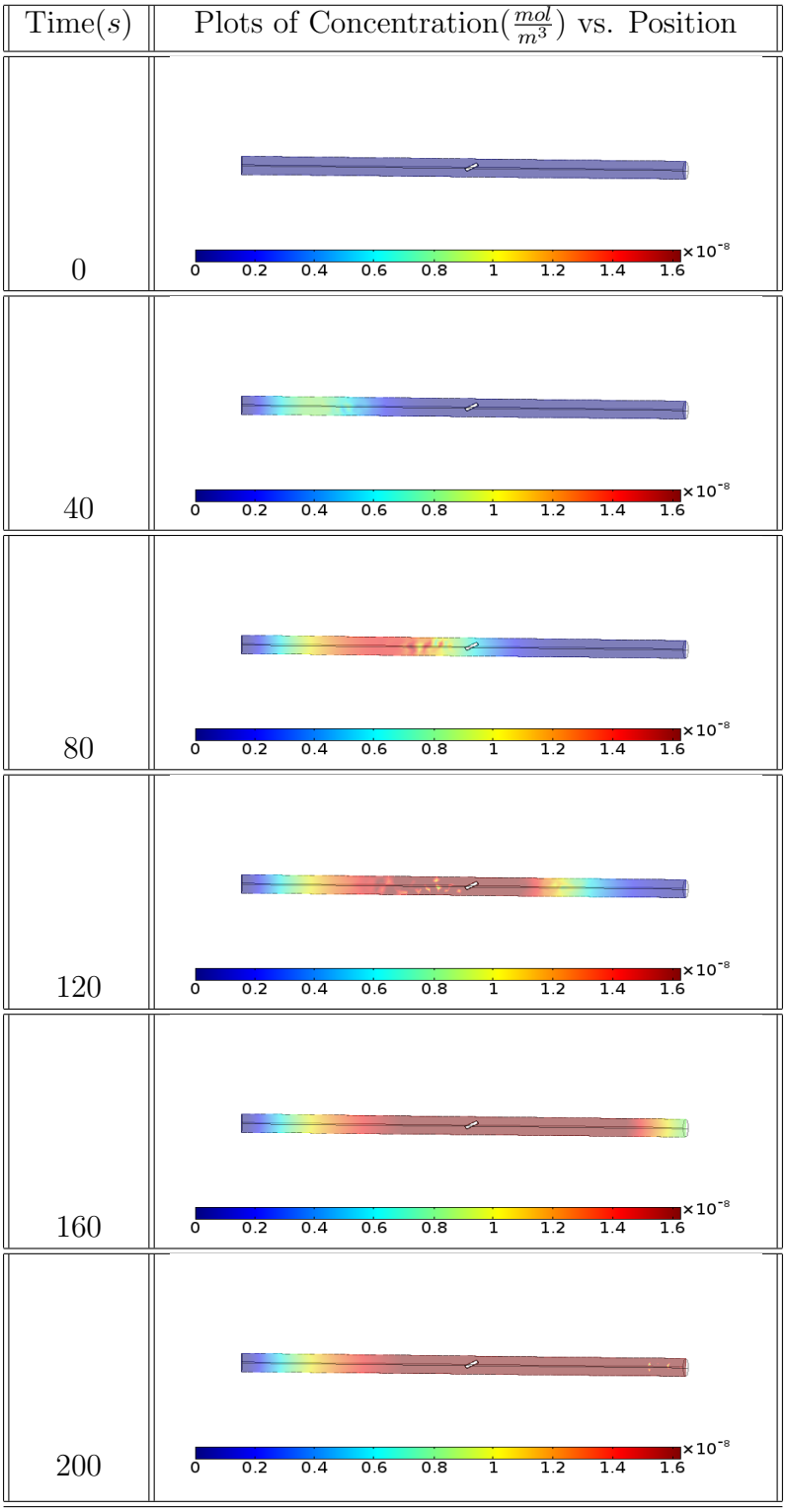

Figure 6.4: C_2H_3 concentration from 0 to 200s at 40 second time intervals.

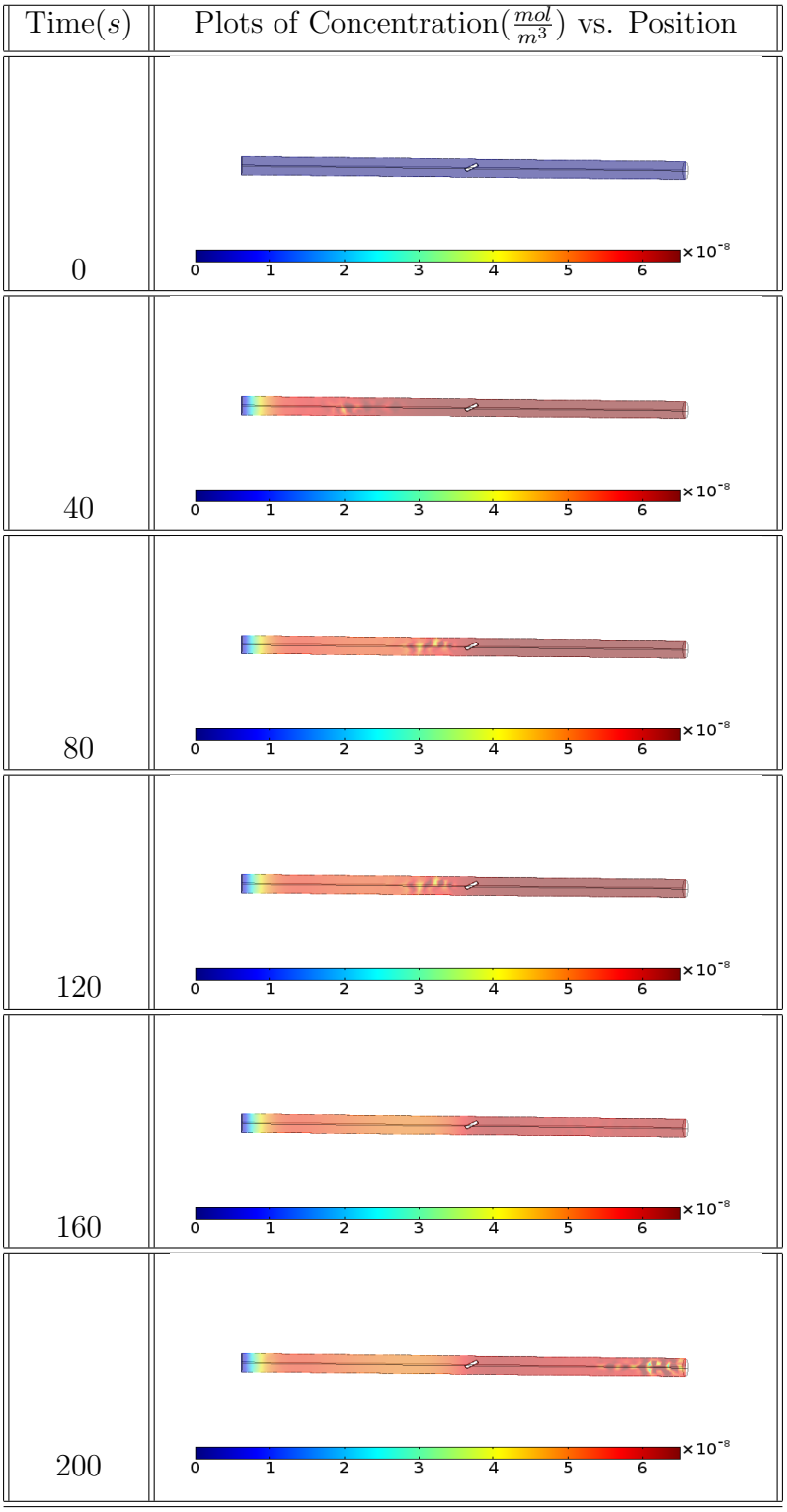

Figure 6.5: H concentration from 0 to 200s at 40 second time intervals.

Time(s)	Plots of Temperature(K) vs. Position
0	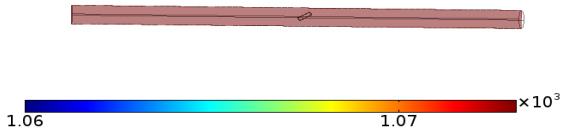
40	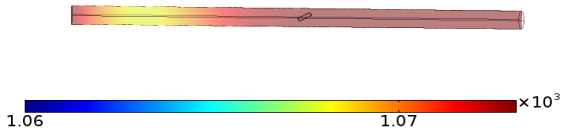
80	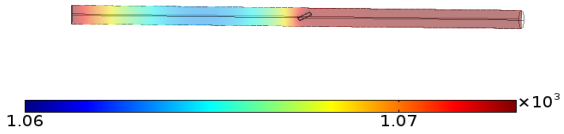
120	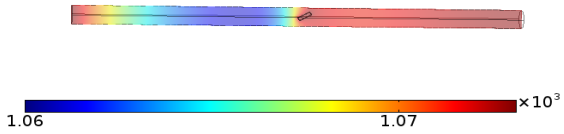
160	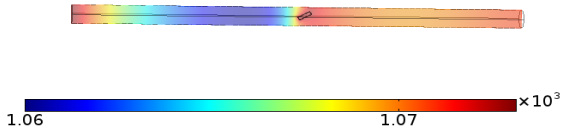
200	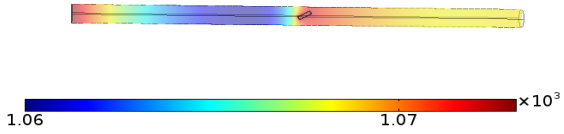

Figure 6.6: Temperature from 0 to 200s at 40 second time intervals.

Time(s)	Plot of Gas-Phase Velocity($\frac{m}{s}$) vs. Position
0	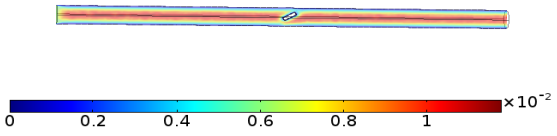

Figure 6.7: Gas-Phase Velocity from 0 to 200s at 40 second time intervals.

Time(s)	Plot of Pressure(Pa) vs. Position
0	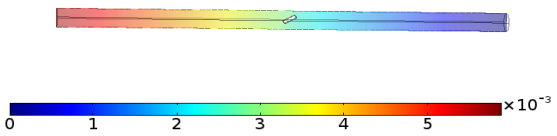

Figure 6.8: Gauge Pressure from 0 to 200s at 40 second time intervals.

Chapter 7

Modeling of a Chemical Vapour Deposition Reactor in 2-D

This chapter describes the first 2-D model as a continuation of the 3-D modeling efforts. The physical description and multi-physics included in the model remain the same; containing Laminar Flow, Heat Transfer, Chemical Kinetics, and Mass Transport. Detailed gas-phase and surface reaction mechanisms have been tabulated in order to generate a plan for the next steps. In order to improve the accuracy of the model, various numerical methods, such as the Backwards Differential Formula and Generalized-Alpha, were researched. 0-D and 1-D simulations were also implemented in order to obtain an understanding as to how easily COMSOL comprehends complicated chemical reaction mechanisms and how well refining the mesh size can work for solving any convergence or accuracy issues.

7.1 Improving the Simulation Accuracy

In highly developed transient simulations for Chemical Vapor Deposition (CVD), many convergence issues may arise. This can be due to discontinuities between boundary conditions and initial values, initial conditions being "too far" from the final results, or an inadequate mesh size. Chemical reactions occur on a very small scale, so incurring the accuracy required to obtain physical results may be computationally demanding. Numerical solvers offer methods to improve aspects such as step-size and relative tolerance, but will not resolve problems which smaller scale meshes improve. Initially, it is difficult to differentiate between Chemistry Interface comprehension and numerical stability. 0-D simulations build a foundation upon which more complicated Chemical Reaction Mechanisms can be implemented. De-

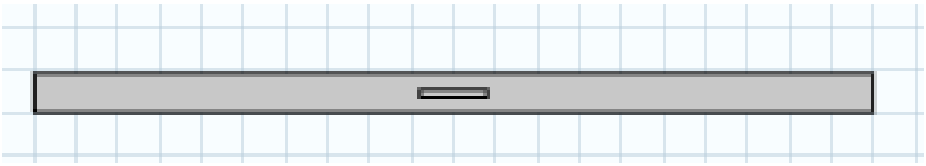

Figure 7.1: 2-D cross-section of the 3-D geometry with the substrate at a 0 degree rotational angle. The length and width of the reactor are 1m and 46mm respectively. The substrate is positioned about its center and the coordinates (x,y) 0.5m and 0.022m where x is along the length of the reactor and y is along the width.

tails such as order of magnitude and concentration absolute positives will then be observed. From here the knowledge base can be extended to a 1-D model which offers more specifics into how meshing will affect the accuracy– potentially flooding out any possible numerical inconsistencies. This comprehensive approach offers insight into whether the mesh or numerical solver should resolve any issues.

7.2 Reactor Geometry

In order to optimize the convergence time, a 2-D cross-section was generated from the 3-D model geometry. In order to further simplify the computational process and obtain more predictable results, the substrate was rotated from the previous -30 degrees (relative to the reactor centerline) to 0 degrees. As will be seen later, this yields a very laminar flow pattern which should be expected given the Reynold's Number calculation (approximately 17) and the usage of the Laminar Flow interface.

The dimensions are the same as before; a reactor length of 1 m and a width of 46 mm. The substrate is still located approximately halfway down the reactor length and halfway up the reactor width. A time-dependent simulation is implemented to study the thermal decomposition of the gas-phase molecular species and to calculate the concentration of molecular species throughout the reactor domain and around the substrate surfaces. A complete physics model includes the coupling of Heat Transfer in Fluids, Mass Transport of Diluted Species, Laminar Flow and Chemical Reaction Engineering modules of COMSOL. Since the 2-D simulation is taken as a cross-section of the 3-D geometry, the boundary conditions remain the same. Due to the transient nature of the simulation, more detail was required in order to optimize convergence and accuracy. The changes will be discussed along with two common numerical methods for transient simulations– BDF and Generalized-Alpha.

7.3 Backwards Differentiation Formula

The Backwards Differentiation Formula (BDF) is a numerical method which is normally utilized for diffusion-type problems. It is utilized to solve initial value problems and takes the general form:

$$y' = f(t, y); y(t_0) = y_0 \tag{7.1}$$

$$\sum_{k=0}^{s} a_k y_{n+k} = h * b * f(y_{n+s}, t_{n+2}) \tag{7.2}$$

where h is the step size, and

$$t_n = t_0 + n * h \tag{7.3}$$

The coefficients a_k and b are chosen so that one can achieve order "s" which is the maximum. Note that for the lowest order, corresponding to s =1, we have the following:

$$a_0 y_n + a_1 y_{n+1} = h * b * f(y_{n+1}, t_{n+1}) \tag{7.4}$$

But, since this is a first order approximation of a derivative, where $\frac{dy}{dt} = h * b * f(y_{n+1}, t_{n+1})$, to achieve $dy = y_{n+1} - y_n$ and $dt = h$, we need the $k = 0$ and $k = 1$ coefficients to be -1 and 1 respectively and for b to be 1. Hence, that we would indeed have the following:

$$y_{n+1} - y_n = h * f(y_{n+1}, t_{n+1}) \tag{7.5}$$

which happens to be the Backwards Euler Formula. This is useful to point out in order to understand the analogy to higher order.

7.4 Generalized Alpha

Generalized-Alpha is a common numerical method used for structural mechanics. In comparison to BDF, it may be preferred due to its improved accuracy. This surplus of accuracy appears because the numerical damping can be controlled much more easily. This implies that convergence may be reached faster in some cases. However, this numerical method is not as stable as BDF. The Generalized-Alpha method is normally derived as follows and was taken from the Negrut et al paper on numerical

integration formulas [2].

Considering a square mass matrix,$M \in \Re^{nxn}$ and generalized coordinates,$y \in \Re^n$

Newton's Second Law implies that for $y'' \in \Re^n$, $My'' = f(t, y, y')$ for $f(t, y, y') \in \Re^n$. Now, for some $z := y' \in \Re^n$ and $a := z' = y'' \in \Re^n$, we can write the following:

$y' = z, z' = a$, and $Ma–f(t, y, z) = 0$. If M is non-singular, we can write the following:

$$a = M^{-1} f(t, y, z) \tag{7.6}$$

A one-step portion of this method implies that for $(t_0, y_0, z_0, a_\alpha) => (t_1 = t_0 + h, y_1, z_1, a_{1+\alpha})$, where the step size is "h", we have:

$$y_1 = y_0 + h * z_0 + \frac{h^2}{2}((1 - 2\beta)a_\alpha) + 2\beta a_{1+\alpha} \tag{7.7}$$

$$z_1 = z_0 + h((1 - \gamma) * a_\alpha + \gamma a_{1+\alpha}) \tag{7.8}$$

$$(1 - \alpha_m)Ma_{1+\alpha} + \alpha_m Ma_\alpha = (1 - \alpha_f)f(t_1, y_1, z_1) + \alpha_f f(t_0, y_0, z_0) \tag{7.9}$$

One particular special case, which is called the Hiber-Hughes-Taylor-Alpha (HHT-Alpha) method is defined as follows:

$$\alpha_m = 0, \alpha := -\alpha_f \in [\frac{-1}{3}, 0], \beta = \frac{(1 - \alpha)^2}{4}, \gamma = \frac{1}{2} - \alpha \tag{7.10}$$

However, these are special cases of the more generalized form:

$$\alpha_m = \frac{2\rho_\infty - 1}{1 + \rho_\infty}, \alpha_f = \frac{\rho_\infty}{1 + \rho_\infty}, \beta = \frac{(1 - \alpha)^2}{4}, \gamma = \frac{1}{2} - \alpha \tag{7.11}$$

where $\alpha := \alpha_m - \alpha_f, \rho_\infty \in [0, 1]$. ρ_∞ is a parameter controlling numerical damping. The minimum at 0 is for maximum damping. This is the parameter controlled within COMSOL called the "amplification for high frequency". In both the BDF and Generalized-Alpha solvers, the time-step size can be altered as well. This will be discussed further in the Results.

7.5 Discontinuities Between Boundary Conditions and Initial Conditions

Within transient simulations it is imperative to be certain that the boundary conditions remain consistent. A common issue is related to the fact that there may be a

mismatch of various inlet and domain values at time $t = 0$. Within the Mass Transport interface, ethylene, argon, and molecular hydrogen are being flowed in at the inlet at a constant rate. Initially, molecular hydrogen is flowed in to flush out any air that may be present within the reactor. This keeps a continuous concentration at the inlet and within the domain, assuming that the concentrations remain the same. When ethylene is flowed in, however, it is assumed that none is present within the domain. Hence, there is a clear discontinuity between the inlet and domain. Similarly, it is assumed that after the hydrogen is flowed in that for an instant in time we keep the gas stationary within the domain to be consistent with the "no-slip" boundaries. This means that due to the necessary inlet flow there is a discontinuity between the inlet and domain conditions at time $t = 0$.

Step functions of the following form are implemented to solve such problems:
$step(t[\frac{1}{s}])$
where t is time in units of seconds and is multiplied by $1[\frac{1}{s}]$ in order to make the input for the step function unitless. This function is then multiplied at the inlet by the value which is desired to achieve in the following way:
The inlet velocity is defined as $(\frac{(vrate_{Ar}+vrate_{C_2H_4}+vrate_{H_2})}{A}) * step(t[\frac{1}{s}])$ where $vrate_X$ is the volumetric flowrate of species X at the inlet and A is the cross-sectional area. Keep in mind that the step function isn't a perfect step function; otherwise a discontinuity would still remain. Hence, a ramping transition zone over time is defined– normally fairly small.

Within the current simulation, the same step function for the ethylene inlet concentration and velocity are the same since the velocity is imported within Mass Transport in order to define inflow. The transition zone is currently around 0.1. In order to be sure that the step function correctly begins to ramp up near 0s, the location of the center of the step function should be half of the transition zone value. Figure 7.2 is a plot of the aforementioned step function. Transition zones that are too small may yield numerical errors whereas transition zones that are too large may yield inaccurate results, but may help with convergence.

7.6 Results of the Study

When beginning the 2-D study, tables were generated with every necessary gas-phase reaction and surface reactions for various catalysts (nickel, iron, or cobalt). The lists are contained in Tables 7.3 and 7.4.

The current study is focused on implementing the gas-phase mechanism efficiently.

Orange = No Troe Form	Cyan = Troe form	units of A assume Temp. is normalized by T_ref = 1K
Gas Phase Reactions	Forward Activation Energy(cal/mol)	Forward Temperature order
H + H + M = H2 + M	0.0	-1
H + H + H2 = H2 + H2	0	-0.6
CH3 + CH3(+M) = C2H6(+M)	654	-1.18
Low Pressure Limit	2763	-7.03
Troe centering	A=0.619	B = 73.2
CH3 + H(+M) = CH4(+M)	536	-0.534
Low Pressure Limit	2440	-4.76
Troe centering	A=0.783	B=74
CH4 + H = CH3 + H2	10840	1.62
CH2 + H2 = CH3 + H	7230	2
CH + H2 (+M) = CH3(+M)	-370	0.43
Low Pressure Limit	590	-2.8
Troe centering	A=0.578	B=122
H + CH2(+M) = CH3(+M)	0	0
Low Pressure Limit	1600	-2.76
Troe centering	A=0.562	B=91

Table 7.1: Example of the Gas-Phase Mechanism list and parameters. Parameters were cited from GRI-Mech 3.0 [4] and the reactions were cited from Gulas et. al.[7]. Note that the Troe Centering parameters refer to the constants used to calculate the fall-off parameter and,hence,the broadening factor. Also note that next to the reactions defined using the Troe Form, in the same row the Arrhenius Parameters for the high pressure limit are included. The Low Pressure Arrhenius parameters were also listed.

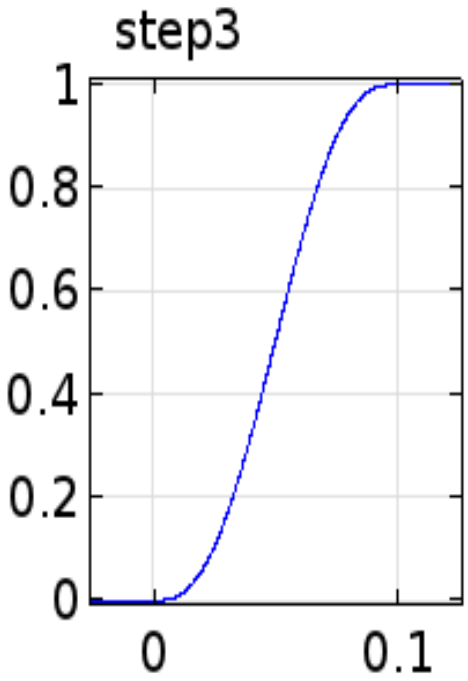

Figure 7.2: Step function centered at 0.05 and a transition zone of 0.1.

Following previous studies in 3-D geometry, attempts to generate similar results within the 2-D geometry proved difficult. Starting with the original three reactions from previous studies, more reactions were included until errors were observed in concentration plots. Figure 7.5 contains an example list of reactions which were started with.

The studies being used run from 0s to 30s with images being taken at 1s intervals. It is important to note that a constant color range is not being used so that the negative concentrations can be seen in the case of changes on the order of 10 or more. Example plots using the above reactions follow in Figure 7.6. The velocity plots show a very laminar flow pattern similar to the flow pattern observed in the 3-D model. The concentrations do not drop below zero for any species at any particular time. However, it is important to note the reasoning for choosing the above reactions to start with. Ethylene (C_2H_4) and molecular hydrogen (H_2) are initial species. This means that following from the initial three reactions one can predict the pathway that the reactions will take. The set listed above is the simplest following left-to-right production. Following the larger set, due to GRI Mech-3.0, many reactions will need to occur in reverse due to the right-hand-side being produced before the left-hand-side species. When beginning to include further reactions (for example: ones which produce CH_X species) the negative concentrations begin to be noticed when plotting

Surface Reactions	Activation Energy	Temperature Order	Forward Frequency Factor
Ni as a catalyst			
$H_2 + S_{Ni} + S_{Ni} => H(s) + H(s)$	0	0	0.01
$H(s) + H(s) => H_2 + S_{Ni} + S_{Ni}$	19409	0	2.55E19
$CH_4(s) => CH_4 + S_{Ni}$	8975	0	8.71E15
$CH_4(s) + S_{Ni} => CH_3(s) + H(s)$	13791	0	3.70E21
$CH_3(s) + H(s) => CH_4(s) + S_{Ni}$	14718	0	6.03E21
$C(s) + H(s) => CH(s) + S_{Ni}$	38506	0	4.56E22
$CH_3(s) + S_{Ni} => CH_2(s) + H(s)$	23901	0	3.70E24
$CH_2(s) + H(s) => CH_3(s) + S_{Ni}$	13224	0	1.29E23
$CH_2(s) + S_{Ni} => CH(s) + H(s)$	23207	0	3.70E24
$CH(s) + H(s) => CH_2(s) + S_{Ni}$	18924	0	4.09E24
$CH(s) + S_{Ni} => C(s) + H(s)$	4493	0	3.70E21
$CH_4 + S_{Ni} => CH_4(s)$	0	0	0.008

Table 7.2: Surface reactions with nickel as the catalyst with forward rate constants in Arrhenius Form. The reactions were cited from Janardhanan et. al. [9].

$2H + Ar = H_2 + Ar$
$2H + H_2 = 2H_2$
$H + C_2H_2(+Ar) = C_2H_3(+Ar)$
$H + C_2H_3(+Ar) = C_2H_4(+Ar)$
$H + C_2H_3 = H_2 + C_2H_2$
$H + C_2H_4(+Ar) = C_2H_5(+Ar)$
$H + C_2H_5 = H_2 + C_2H_4$
$C_2H_4(+Ar) = H_2 + C_2H_2(+Ar)$

Table 7.3: Table of reactions used initially

such as in Figure 7.8.

Following the standard procedure of implementing the "max" function for the Mass Transport source terms and a "Flux Danckwerts" boundary condition in order to avoid negative concentrations from species acting as sinks, the values still remained. Both the BDF and Generalized-Alpha numerical methods were implemented in order to figure out if these negative concentrations were a numerical issue or an issue of COMSOL not comprehending reactions which occur backwards initially.

A "normal" sized mesh was commonly used during the following process. First, the relative tolerance was lowered in order to improve accuracy. Within BDF, a "free" solver can be implemented which tells COMSOL to automatically determine a time-

$H + C_2H_4 = C_2H_3 + H_2$
$H + C_2H_5(+Ar) = C_2H_6(+Ar)$
$H + C_2H_6 = C_2H_5 + H_2$
$CH_2 + CH_4 = 2CH_3$
$CH_3 = H + C_2H_5$
$C_2H_2 + H(+Ar) = C_2H_3(+Ar)$

Table 7.4: Additional set of reaction including ones which incorporate CHX species. Reactions containing such species should occur in reverse before forward based off of the set-up.

step size which will satisfy the relative tolerance being lower than the relative error. Other options are available such as "strict" and "intermediate" which allow the user to control the time-stepping within the "time-range" definition. As a reminder, the "time-range" is utilized to define a range over which images will be created at a particular time-interval. This being more complicated than the "free" solver was motivation for not using these methods. The Generalized-Alpha method proved to be useful as well, but not quite as much as the BDF-free. "ρ_∞" within the Generalized-Alpha method is called "Amplification for High Frequency" in COMSOL and values can be selected between 0 and 1. Commonly, values above 0.5 yield more accurate results since there is more damping. However, lower values yield easier convergence due to lower damping.

While working with both solvers, a common issue was discovered: in order to achieve convergence, unrealistic low values for the "Amplification for High Frequency" and unrealistic high values for the initial time-step and maximum time-step were needed for convergence. In order to simplify the process, the BDF solver was chosen since it is more common to use for diffusion-type problems and analogous errors were repeating while using the Generalized-Alpha solver. At this point, in order to diagnose the issues, varying physics-controlled mesh sizes were used. It was found that an "extremely fine" size helped to achieve convergence, but negative concentrations were observed.

In order to analyze the issue of negative concentration, a "double-check" method was implemented. A 0-D simulation was generated in order to double-check that COMSOL is indeed comprehending the complex gas-phase reaction mechanism. Then, a 1-D simulation was created in order to test the effects of mesh size on improving accuracy.

7.7 0-D Simulation

The 0-D simulation was created through including a stationary plug flow study with 47 gas-phase reactions of interest from the complete set. A constant temperature of 800 Celsius and a pressure of 1[atm] internally and 0[atm] externally (as a simpler reference), along with no external heating, were utilized for the set-up. A simple set-up using argon as the solvent and a step over "volumes" from 0 to 1 by 0.1 yielded concentration plots(Figure 7.9).

These plots show that no concentration should drop below zero. Hence, COMSOL is correctly comprehending the gas-phase mechanism inputs. This implies that the issue is inherent to the numerical approximation. A 1-D set-up offers insight into this topic.

7.8 1-D Simulation

The geometry used for a simple 1-D model was a line segment from 0 to 1 meter. Granted, this ignores the effect of including a substrate but gives a general idea of what to expect. Chemistry, Mass Transport, and Heat Transfer interfaces were all included along with the aforementioned 47 gas-phase reactions. Within 1-D simulations, only Darcy's Law is available for fluid flow. In order to simplify the computation process, a fluid flow interface was ignored. However, COMSOL has the ability to define the velocity field magnitude within the Mass Transport and Heat Transfer Interfaces. The same magnitude used within the 2-D simulation was included. One could have implemented a stationary solution with a stationary plug-flow solver, but it analogous to utilizing a time-dependent set-up. In order to remain consistent with the 2-D simulation, a time-dependent simulation was used along with the 0 to 30s by 1s increments time range. The following concentration plots were generated while using an "extremely fine" mesh size.

Once again, negative concentrations were observed. From the numerical method 2-D study, it was shown that one cannot rely on the numerical solver to resolve the negative concentration phenomenon. Hence, a user-controlled mesh was generated. The default maximum element size for an "extremely fine" setting is approximately 0.01. After dropping this value to 0.009, the negative concentrations were no longer present as seen in the previous plots.

This study showed, in a much less computationally extensive manner, that the physics-controlled mesh in the 2-D study needs to be changed to a user-controlled

mesh with a much lower maximum element size.

7.9 An Attempt to Improve the 2-D Simulation

Focusing the results of the previous studies on the 2-D model, showed that indeed a smaller maximum element size within the user-controlled mesh helps. For the time being, a smaller reaction set is being used before jumping to the set of 47 reactions and then to the complete set. The most recent study implemented a maximum mesh size of 0.007. Smaller mesh sizes will be analyzed since in the future. However, it was discovered in one simulation run that a maximum element size of 0.0001 is much too small and leads to COMSOL crashing. Plots from using the 0.007 element size are included in Figure 7.11.

7.10 A Quick Discussion of the Plots

An important aspect of these simulations is to determine the validity of the plots being generated. Since the velocity profile being generated is in accordance with the previous 3-D model runs, it appears that there is a consistency. Due to the order of ten calculations in "m/s" for the inlet velocity, the domain values appear to be reasonable, especially around the substrate since there is a smaller cross section area the gas is moving through. Indeed, one should also observe an increase in pressure near the substrate which is also noticed. The plots being focused on, however, are the concentration profiles. With the refined mesh element size, the outputs show that for most species the negative concentrations disappear. The remaining species concentrations, along with the negative pressure values, should be able to be corrected with smaller element sizes.

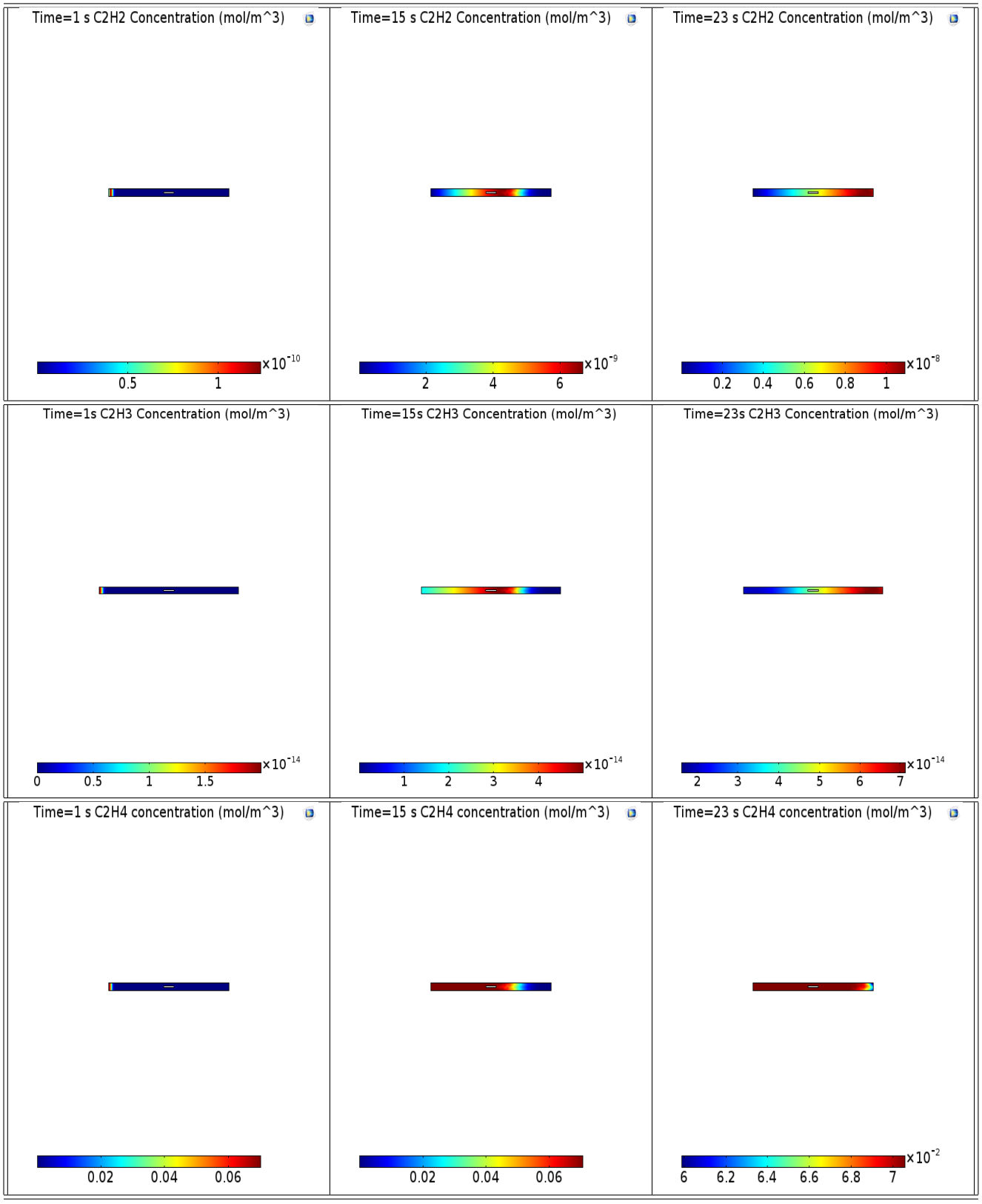
Time=1 s C2H2 Concentration (mol/m^3)
×10^-10
0.5
1
Time=15 s C2H2 Concentration (mol/m^3)
×10^-9
2
4
6
Time=23 s C2H2 Concentration (mol/m^3)
×10^-8
0.2
0.4
0.6
0.8
1
Time=1s C2H3 Concentration (mol/m^3)
×10^-14
0
0.5
1
1.5
Time=15s C2H3 Concentration (mol/m^3)
×10^-14
1
2
3
4
Time=23s C2H3 Concentration (mol/m^3)
×10^-14
2
3
4
5
6
7
Time=1 s C2H4 concentration (mol/m^3)
0.02
0.04
0.06
Time=15 s C2H4 concentration (mol/m^3)
0.02
0.04
0.06
Time=23 s C2H4 concentration (mol/m^3)
×10^-2
6
6.2
6.4
6.6
6.8
7

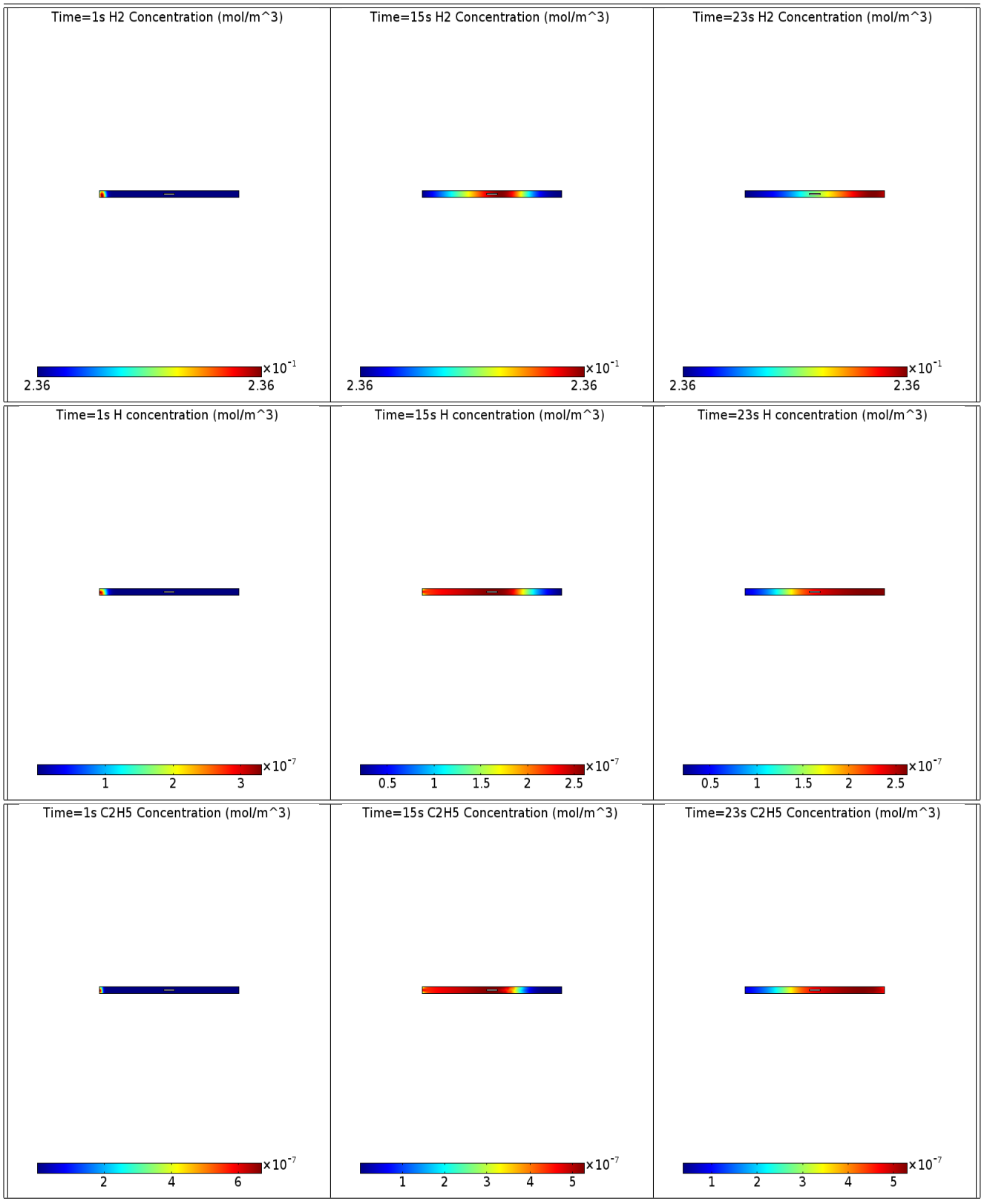

Figure 7.3: Plots of concentrations in $\frac{mol}{m^3}$ for 6 species involved in the aforementioned reactions. Images were taken from 1s, 15s, and 23s to show data from a broad range in case any phenomena would appear throughout the process.

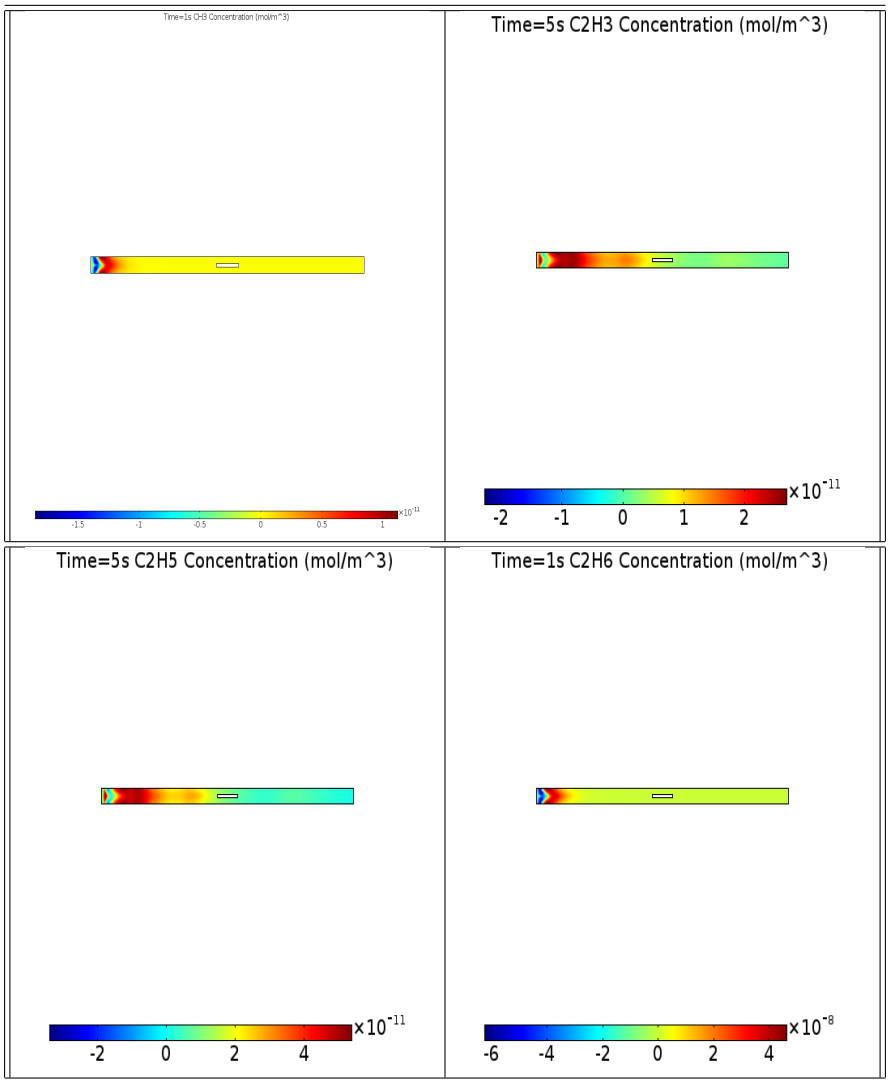

Figure 7.4: Examples of species concentrations dropping below zero at time t=1s and t=5s. Note the drop in concentration below zero in each example.

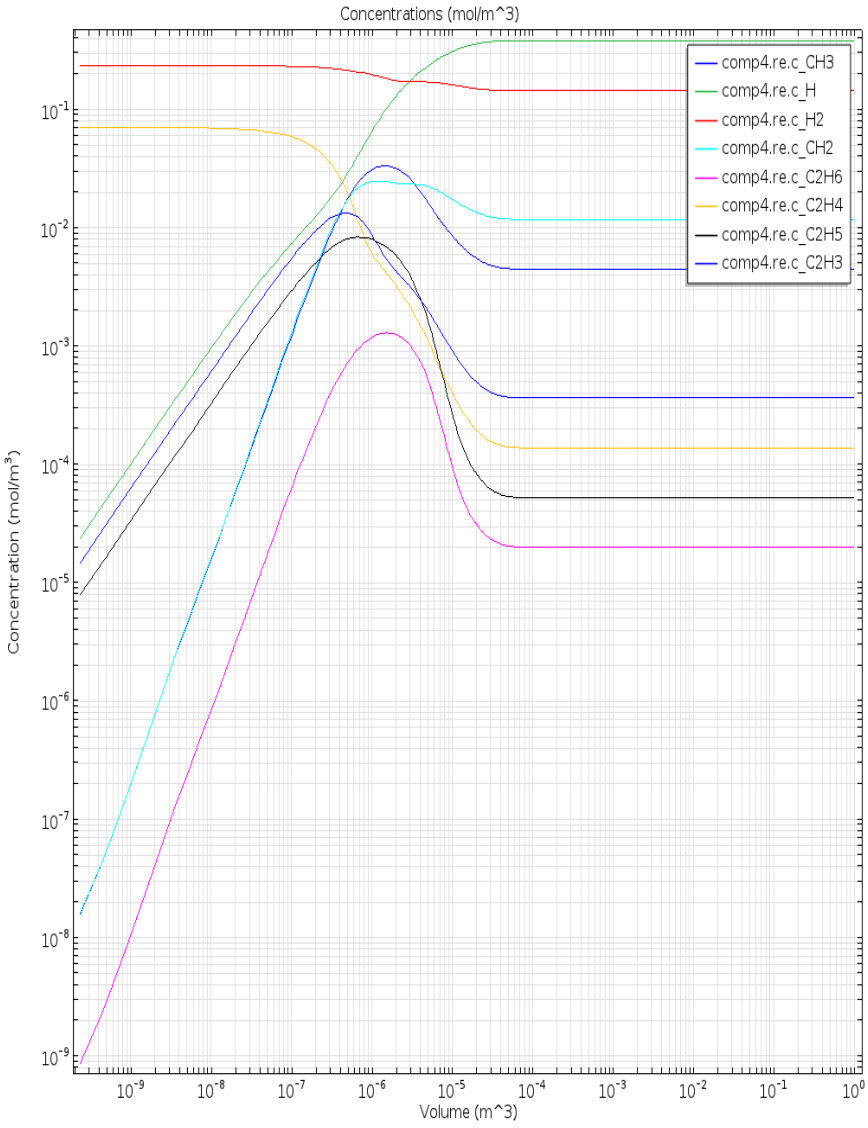

Figure 7.5: Sample concentration plots of species. In order to avoid incoherent plots from too many species being plotted, 8 were chosen as a comparison to previous plots. Specifically, note how C_2H_6 does not drop below zero like it did previously around 1s. Stationary plug flow steps over volume, but this is analogous to time-stepping.

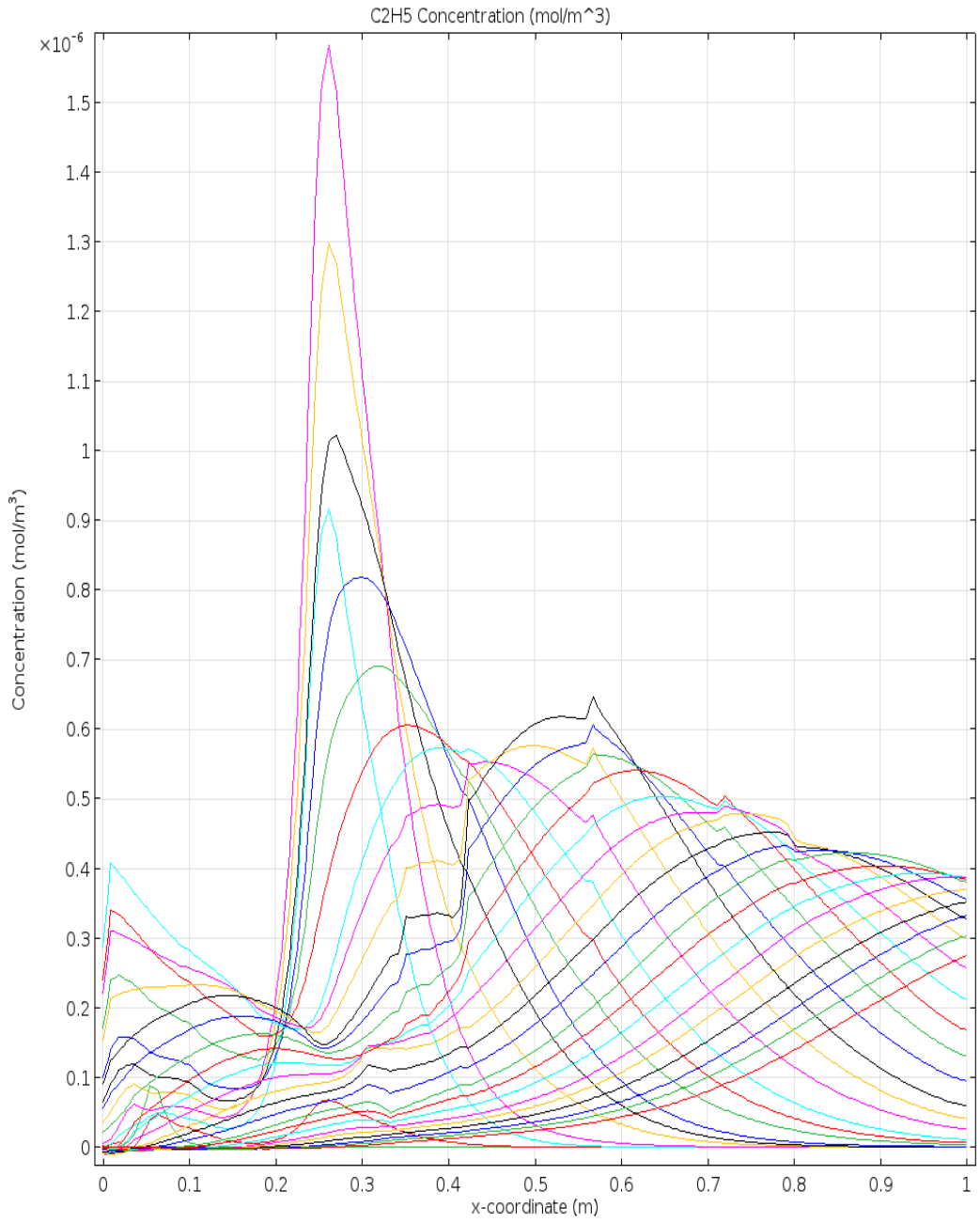
C2H5 Concentration (mol/m^3)
×10^-6
1.5
1.4
1.3
1.2
1.1
1
0.9
0.8
0.7
0.6
0.5
0.4
0.3
0.2
0.1
0
Concentration (mol/m^3)
0
0.1
0.2
0.3
0.4
0.5
0.6
0.7
0.8
0.9
1
x-coordinate (m)

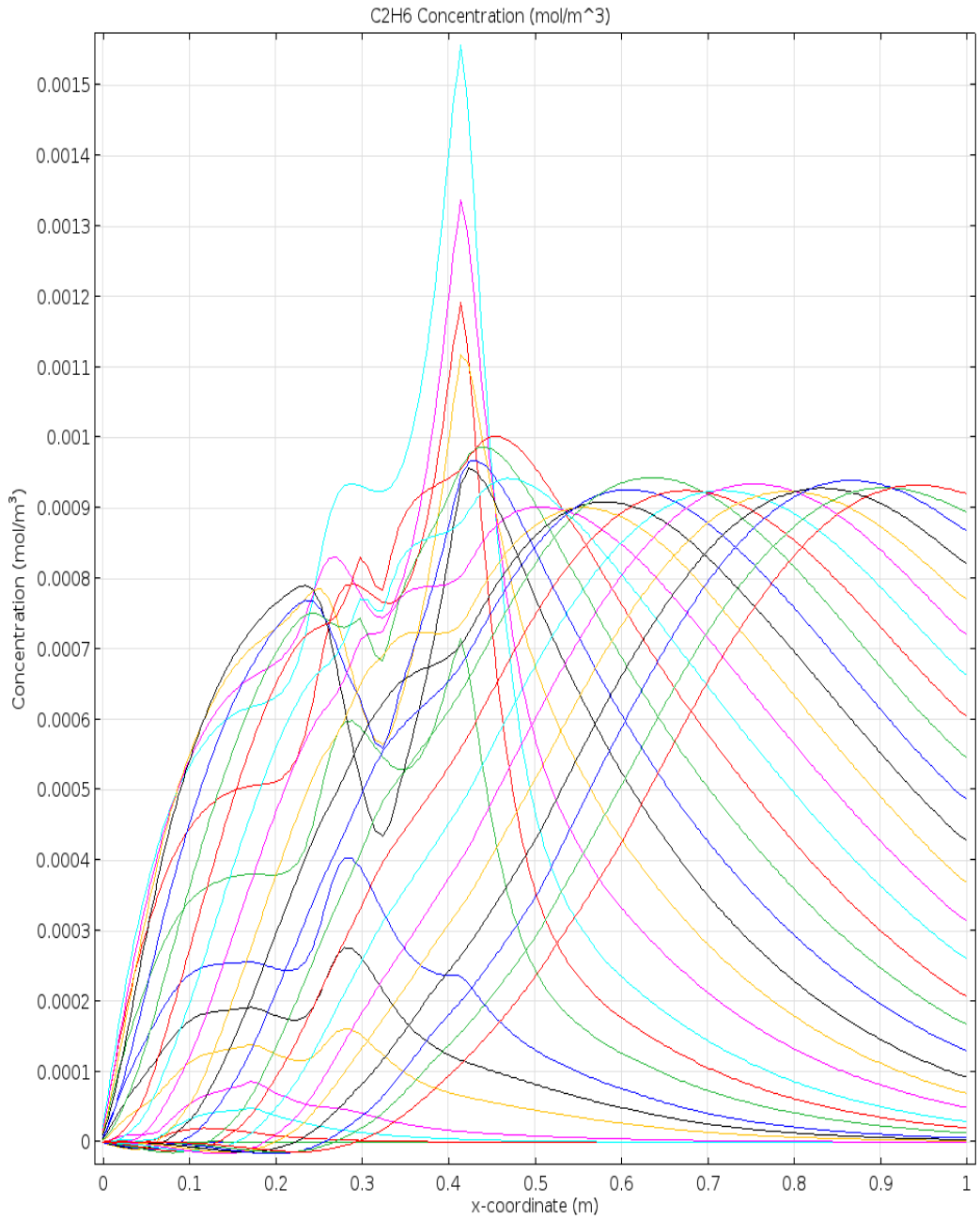

Figure 7.6: Concentrations of C_2H_5 and C_2H_6 vs. x-coordinate. The many lines in the plots denote the concentrations at various times at 1s intervals between 0s and 30s. Note the slight drop below zero. This is artificial due to numerical errors. The element size used to generate these was 0.009. When using 0.01, the negative concentrations were pronounced.

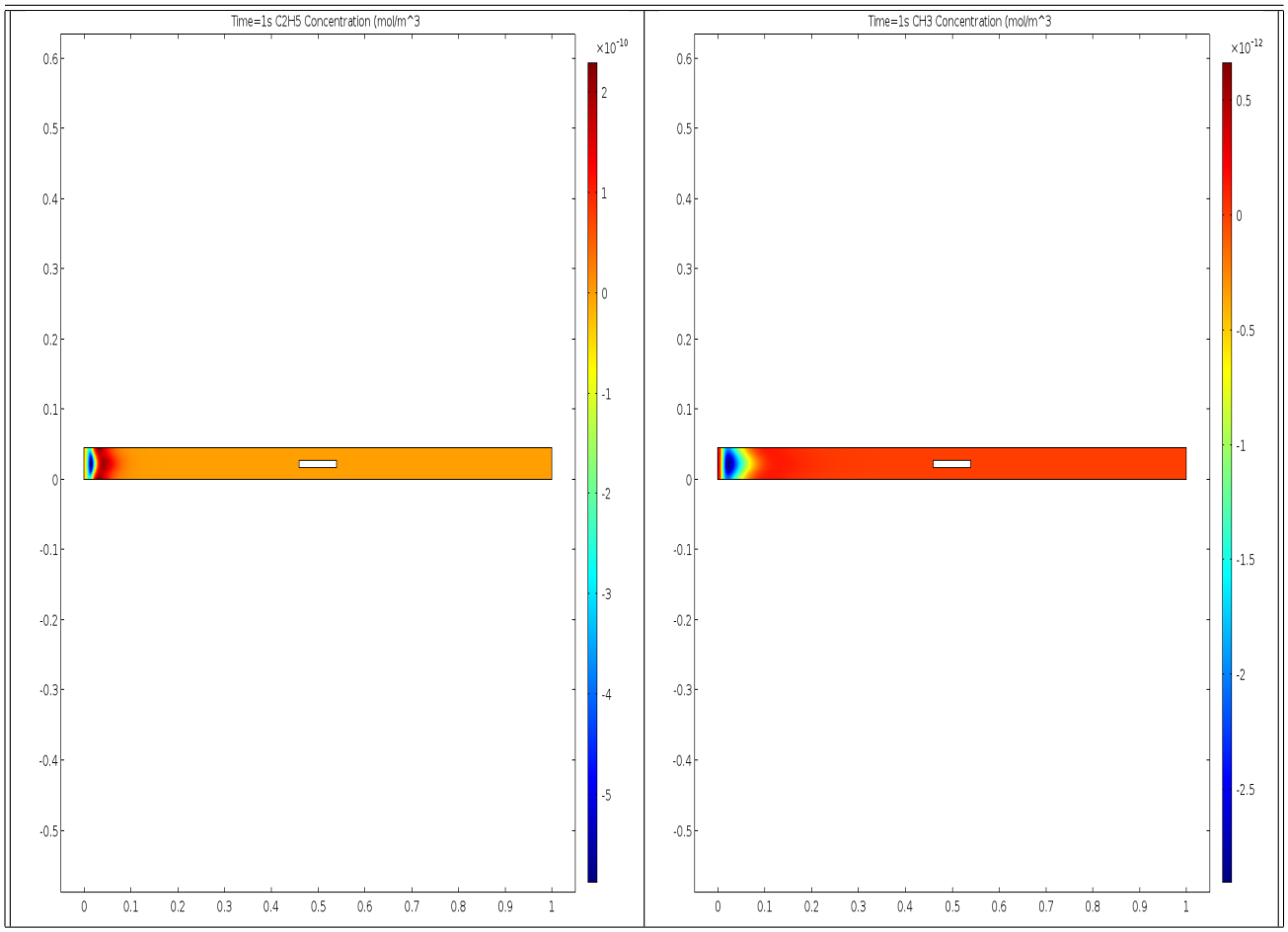

Figure 7.7: 2-D concentration plots of CH_3 and C_2H_5 at t = 1s. Note that the concentrations drop below zero. Initially, before using a mesh element size of 0.007, these negative values were much more pronounced. They were approximately -8E-12 for CH_3.

Chapter 8

Switching to a 2-D Stationary Model for Optimization

This chapter constitutes the description of 2-D stationary results for a set of 32 gas-phase reactions in a cylindrical reactor. Complications arose in the transient method due to non-optimized boundary conditions, computation expense, etc. Hence, analysis of mesh refinement contributing to convergence led to the discovery of limitations in other aspects of the simulation such as: Troe form not being the optimal choice for chemical kinetics, mismatched velocity conditions, and incorrect use of initial conditions for concentrations of chemical species.

8.1 Approach to the 2-D Stationary Model

When first switching to the 2-D stationary solver, convergence issues began to arise due to a lack of optimization in the use of the numerical method and initial conditions for the concentrations. Since there was a switch from a transient solver to a stationary solver, it is important to note that simpler boundary conditions were considered in order to avoid the complexity of the previously utilized functions ("max" for reaction rates and "step" functions for inlet conditions mismatched with initial values) to see if the model could be self-consistent. More specifically, there was testing to see if negative concentrations would arise and step-functions were ignored through setting the inlet and initial conditions to be the same values. Unfortunately, it was observed that negative concentrations did appear, even through the use of the "max" function for the reaction rates.

In order to analyze this specific issue, it was decided that stepping back to a 0-D study would elucidate any issues with the chemistry if they were present. After such

a study, a 1-D study would be generated in order to get a conceptualization as to how refined the mesh would need to be in 2-D to remove the negative concentrations. The latter of these two studies would show that the negative concentrations are a fabrication due to numerical error. Hence, the 0-D study illuminated that negative concentrations indeed did not appear.

Due to the simplicity of such a model, the decision was made that the chemistry was not generating the problems (at this point a relevant 32 reactions were successfully added which will be discussed). After an attempt in a 1-D transient study (plug flow stationary solver and transient solver are essentially the same in 1-D), the presence of negative concentrations in the initial study were observed. Once the mesh size was tweaked, it was noted that quite a fine mesh was required to notice an improvement. On the other hand, both physics controlled and user controlled meshes were being considered. Since the physics controlled mesh element sizes only get so small (approximately 0.01m), a limit was discovered which would optimize numerical accuracy and avoid computational expense. This value was around 0.001m in 1-D and greatly helped in the reduction of the number of negative concentrations being present. Hence, this approach implied that a user controlled mesh may be necessary in 2-D in order to remove any negative concentrations.

Due to various errors occurring, it was discovered that it may be useful to implement a segregated solver to improve convergence. Such solvers attempt to solve each physics interface separately and then incorporate the individual solutions to formulate a final solution. It was observed that convergence improved greatly after implementing said solver. Also, since a different mesh size was needed in 2-D , it was recorded that an optimal mesh element size was around 0.00099m along with an optimal relative tolerance of 0.0001. After running a study, it was discovered that negative concentrations were still present but only observable when one zooms in on the inlet. This seemingly showed that the negative values are numerical since the mesh can only resolve so well due to sharp corners at the inlet.

The relevant 32 reactions were then included and convergence was obtained, but it was noticed that odd behavior in the velocity and concentration plots (negative values) could be generated if the substrate was rotated from 0 degrees. This implied that it was necessary for the time being to remove the angle in the substrate. Interestingly enough, convergence greatly improved as well as the resolving of the velocity profile and concentration plots. Further, in order to simplify the process the substrate was removed all together in order to run tests to make sure that chemistry would be optimized without error due to computation about sharp edges in the geometry.

At this point, the concentration profile of amorphous carbon, C, was very uninformative. It was constant throughout the reactor at about $10^{-15}[\frac{mol}{m^3}]$ which is actually the value of the "eps" constant which every species was initialized to, other than C_2H_4, H_2, and A_r, so that the initial conditions would be closer to the final results and help with convergence. However, intuitively there should be some gradient. A CHEMKIN simulation was performed on the side by Dr. Amit Sharma in order to analyze what the approximate equilibrium concentration should be in a batch reactor with the reaction set of interest. It was shown that around $10^{-22}[\frac{mol}{m^3}]$ may be reasonable. This made it apparent that the value of "eps" was too high to resolve the gradient illuminating formation. A value of "eps^2" was implemented for every species other than the initial ones since it was known that this value wouldn't initialize amorphous carbon higher than the approximate equilibrium concentration which should be observed. A new run showed that the amorphous Carbon concentration did peak at around $10^{-22}[\frac{mol}{m^3}]$.

At this point, focus was put towards the generation of plots of the concentrations of all species in order to perform theoretical equilibrium calculations and try different initial temperatures and velocities. There was also a latent concern as to whether the $10^{-22}[\frac{mol}{m^3}]$ value for amorphous Carbon was too small and whether or not the small drop in concentration of C_2H_4 was accurate. The reasons being are that it was thought C_2H_4 cracking should be more efficient and with a concentration of about $10^{-22}[\frac{mol}{m^3}]$ of amorphous carbon this amounts to approximately 60 Carbon atoms in a $1[m^3]$ volume. Since the length of the reactor being used in 1[m] with a width of 46mm, the volume would be much smaller than $1[m^3]$ and hence the total number of Carbon atoms in the reactor domain in the final state would be much smaller than 60. Dr. Ahmad E. Islam (WPAFB) has claimed that experimentally these values are not observed. Hence, this was grounds to look further into theoretical equilibrium calculations.

Before going into further detail about equilibrium calculation comparisons, the analysis of changing both temperature and velocity should be noted. It was discovered that at slightly higher and lower temperatures predictable results occurred. It should be expected that at higher temperatures from 800C that C_2H_4 cracking will become more efficient and the opposite for smaller temperatures than 800C. Although this was observed, it was also observed that the initial conditions were very unstable so that when initial conditions were drastically far away from 800C a lack of convergence would ensue. This could mean that there is a lack of optimization in the numerical setup, or there is something incorrect with the model. However, at this

point there weren't any obvious changes which needed to be made. Next, the change in velocity was tested in order to test the hypothesis that decreasing the inlet velocity should increase production of amorphous Carbon. Indeed, when the velocity was decreased by a factor of 2 it was observed that there was more efficient decomposition of C_2H_4 and, hence, there was more production of amorphous Carbon. This result is important because it illuminates the importance of initial conditions on equilibrium values.

At this point, it was imperative to pursue theoretical equilibrium concentration calculations in order to see if the values being obtained are indeed reasonable in both the CHEMKIN and COMSOL simulations. This analysis will follow in the next section.

8.2 Theoretical Equilibrium Calculations

There are various standardized methods which can be used in order to perform on-the-fly theoretical equilibrium concentration calculations. The method which was decided upon was the Initial, Change, Equilibrium (ICE) table method due to the information which can easily be obtained from GRI-Mech 3.0 [4]. More specifically, this method relies upon knowing the value of the equilibrium rate constant at a particular temperature which can be approximated using the temperature ranges and corresponding values of the rate constant. To begin with a simple example, the C_2H_4 decomposition reaction was chosen.

Since we have already defined initial concentrations for both H_2 and C_2H_4 from pre-defined volumetric flowrates in SCCM and using the ideal gas law to find molar flowrate and, hence, the concentrations we can set up the ICE table as follows:

First, one needs to derive the form of the equilibrium constant so one can tell which species and/or products will be relevant to the calculation:
By definition,

$$K_{eq} = \frac{[H_2][C_2H_2][M]}{[M][C_2H_4]} \tag{8.1}$$

and, hence,

$$K_{eq} = \frac{[H_2][C_2H_2]}{[C_2H_4]} \tag{8.2}$$

which shows that [M] doesn't affect equilibrium constant, so species M does not need

	C_2H_4	C_2H_2	H_2
Initial	0.0706	0	0.2348
Change	-x	+x	+x
Equilibrium	0.0706-x	x	0.2348+x

Table 8.1: ICE Table to find equilibrium concentrations of participating species.

to be included in the ICE table with concentrations in units of $[\frac{mol}{m^3}]$. Since there is only one mole of each species, the coefficients of the change variable, x, need only be "1".

Now, referring to GRI-Mech 3.0 for this reaction one can argue that the equilibrium rate constant should be approximately $0.1[\frac{mol}{m^3}]$. Checking units from (8.2) verifies that this is indeed reasonable [4].
Now, the following equation can be set up:

$$\frac{x(0.2348+x)}{0.0706-x} \tag{8.3}$$

and x can be solved for which yields,

$$x = -0.354704, x = 0.0199039 \tag{8.4}$$

both in units of $[\frac{mol}{m^3}]$.

But, it can be observed that if x is negative then the equilibrium concentration of C_2H_4 will be larger than the initial concentration, which cannot be the case, so the positive value is utilized, which implies at equilibrium:

$$[C_2H_4]_{eq} = 0.0507[\frac{mol}{m^3}] \tag{8.5}$$

$$[H_2]_{eq} = 0.2546[\frac{mol}{m^3}] \tag{8.6}$$

$$[C_2H_2]_{eq} = 0.0199[\frac{mol}{m^3}] \tag{8.7}$$

These values are very important, because they offer a means to check the validity of the chemical kinetics being utilized within COMSOL.

8.3 A 0-D Comparison of ICE Table Results to Batch Reactor Simulation

In order to generate a reasonable comparison, an initial check was performed keeping all of the reaction kinetics using TROE form, using 0.1 as the equilibrium constant, temperature being set at 1073.15K(800C), and Argon being utilized as the third body species (M). A transient solution was utilized as well since intuitively when time is ramped to a large enough value the concentrations should flatten out at a steady state which would imply equilibrium has been achieved. After taking time to a sufficiently large value in order to achieve constant concentrations results were gathered(Figures 8.2 and 8.3). Note that whenever Arrhenius Form is being utilized from a CHEMKIN file, imported reactions (which have solely been used from GRI-Mech 3.0), abide by the high pressure rate limit of the rate constant.

It can be noticed that the Troe Form kinetics are not accurately capturing the results which should expected, but the high pressure rate limit in Arrhenius Form does indeed capture (almost exactly) the results predicted from the ICE table. This was a motivation for the switch to Arrhenius Form.

8.4 Redefining the 2-D Model

Once the discovery was made that the Troe Form wasn't being implemented correctly in COMSOL, a switch to Arrhenius Form was made within the 2-D model. Many errors had occurred with regards to adding multiple reactions and, hence, similar methods as was done previously had to be rotated through once again. The methods are: adding reactions one at a time to see if the problem could be illuminated, testing different numerical methods such as "fully coupled" and "segregated", using "eps" or "eps^2" for the initial concentration of species which are not being flowed in, and checking that theoretical equilibrium calculations match the 2-D results. Through various trial-and-error runs, it was discovered that there was an inconsistent boundary condition within the Laminar Flow interface. Due to the current simulation being stationary, it is imperative that the boundary and domain (initial) conditions are in accordance. This being in opposition to the time-dependent solutions. Although within a time-dependent study the conditions don't have to match exactly, one would have to utilize step-functions which is not necessary in this case. Instead, there was an inlet velocity defined in previous chapters(sum of volumetric flowrates of inflowing species divided by cross-sectional area) and a mismatched initial condition(zero ve-

locity in the domain). Theoretically, the difference is very minute between defining a zero domain velocity condition and letting the inflowing gas to force the other gases to a laminar velocity profile. The only difference should be the wait for steady state to approach. However, COMSOL doesn't handle the aforementioned inconsistent setup very well.

Once the change was made with this condition, "eps^2" was implemented for initial conditions(not that "eps" can't work for convergence, it is that its use doesn't help generate accurate concentration profiles), and the reactions from Figure 8.4 were added one-by-one. Concentration, velocity, and temperature profiles were generated as well as follow-up tests.

Before displaying the final results, it is important to note that tests were also performed in order to analyze how consistent a small set of reactions would be with equilibrium calculations. A quick recorded test was performed using only the C_2H_4 decomposition reaction. More tests are needed in order to fully clarify that the results are indeed consistent, however reasonable they may seem.

Hence, one can notice that the max concentration for H_2 and the minimum concentration for C_2H_4 do not exactly match the concentrations one should expect from the theoretical calculations. As was discussed previously, a velocity effect has been studied which is the following hypothesis: Will the minimum concentration drop if the inlet and domain velocities are dropped? Intuitively, this makes sense since as a lower velocity would increase the residence time of each gas in the reactor which will increase the efficiency of C_2H_4 cracking. The results after dropping the velocity by a factor of 10 are included in Figures 8.7 and 8.8.

Another important result to consider is this velocity effect in accordance with the fact that due to no slip conditions at the boundaries there is indeed a velocity gradient along the vertical diameter of the reactor. Hence, since there is a zero velocity at the surface of the reactor one should see a lower concentration along points lying at the same x-coordinates in comparison to y-coordinates along a line connecting said surface points also at the same x-coordinate(specifically for C_2H_4). Since it is nearly impossible to determine the answer from previous plots which have been created, equi-concentration contour plots were generated in order to perform a reasonable analysis(Figure 8.9).

Indeed, one can notice the velocity effect along the vertical diameter. These results show how important the initial conditions are when defining the chemistry and physics. One can account for the difference from the theoretical equilibrium calculations with a change in the residence time of the gas species. There needs to be

more analysis along the lines of testing the validity for multiple reactions.

8.5 Results of this Study

After performing the previously discussed tests, the final results were collected for the concentration profiles of each species, the velocity profile, and the temperature profile. One will be able to notice that the velocity profile is similar to that of profiles generated previous chapters. Also, the reason the analysis of velocity affecting the concentrations of species is important is due to the fact that the results show a very small concentration for amorphous carbon along the reactor. It just so happens that the effect accounts for this change as well.

As one can see in Figure 8.10, most of the plots show an increasing gradient of concentration along the reactor. This is intuitive since nearly a 0 concentration is being started with for every species and are producing them through the cracking of C_2H_4. Of course there is a depletion of every species due to participation of the reactions. This can account for smaller concentrations than expected. Also, it can noticed that the velocity profile is quite predictable due to the laminar pattern seen across the reactor as well as a zero velocity along the surface generating a gradient towards the center of the reactor. Lastly, when looking at the temperature profile one can see a higher temperature along the inlet and the surface of the reactor, which corresponds to the initial temperature of 1073.15K. However, the temperature along the domain of the reactor drops which can be explained due to endothermic reactions taking place (as discussed in previous chapters). As was discussed earlier, the equilibrium concentration of amorphous carbon($a-C$) was tested against theoretical results for a couple of simple reactions. This was done in order to see if the velocity effect could be reproduced and account for the extremely small concentration of $a-C$. It was observed that the effect remained consistent.

The limitation of the current model is that it does not incorporate surface reactions. Surface reactions are important because they can determine how subsequent species will react with the surface material. Amorphous carbon is of great interest, because the aforementioned concentration gradient test should be utilized to check for consistency between the number of amorphous carbon atoms observed to adsorb on the reactor surface in the simulation and in the experiment. Specifically, the simulated concentration of $a-C$ is on the order of $10^{-20}[\frac{mol}{m^3}]$, whereas the predicted concentration is on the order of 10^{-14}. The thought is that since surface reactions haven't been implemented there won't be a build-up of $a-C$ on the surface and,

hence, the total concentration of it on the reactor surfaces will be a gross underestimation of the realistic value.

Also, reactions including singlet-state species (as well as one other gas-phase reaction) have been left out. The other reaction was left out since convergence issues arise when it is included. Further studies have been performed in order to understand why this is the case. It was thought that since the activation energy could be very small (negative) or the frequency factor could be very large to yield a small reaction rate, there must be an implementation of a very small mesh size or step size. However, there were inconsistencies with the inclusion of the ethylene decomposition reaction which had the largest rate constant at the temperature of $800C$. This led to the motivation to reduce the chemical reaction mechanism since the numerical solver was not able to resolve the problem. The aforementioned reaction does not greatly affect the creation of a-C. Since only GRI-Mech 3.0 reactions have been implemented due to simplicity of implementation due to CHEMKIN import, one can refer to the previous table including the complete reaction mechanism and surface reactions to note the missing reaction.

A goal of the project is to reduce the reaction mechanism in order to simplify the process. In order to do so, a diagram displaying the most immediate pathways to $a-C$ was created. This verified the process of eliminating the reaction. Future work must be done in order to reduce the mechanism further.

It is also imperative to mention that further studies have been performed in order to test that theoretical equilibrium calculations match up with the results from multiple reactions being included(relative to the simple test using only ethylene decomposition). A few tests have been performed for a couple reactions through taking the equilibrium results for C_2H_4 decomposition and $2H + Ar <=> H_2 + Ar$ in order to have initial conditions for reactions including amorphous Carbon. These tests proved to be consistent.

The consistency of the simulation with the theoretical results is showing a promising future for the project since COMSOL is accurately generating predictions which are nearly being predicted. There are a few discrepancies (which have been discussed) between the simulation and experimental results. However, these can be accounted for through tweaking boundary and initial conditions. The velocity effect is an example which has been used to display any differences between the 0-D and 2-D results. However, the 0-D results are still more comparable to the 2-D simulation. The results of 0-D essentially describe the theoretical equilibrium concentrations for multiple reactions. These are indeed in accordance with simulations performed previously in

CHEMKIN.

Since literature has been gathered for surface reactions, the set using Nickel as the catalyst is of interest. Once efforts have been provided to finalize the reduced gas-phase mechanism, the supported substrate can be redefined in the COMSOL geometry and then surface reactions can be included at the internal boundaries of the reactor. This will account for the difference in the overall production of $a - C$ due to soot formation and yield a method for measuring the concentration of adsorbed carbon along the surface of the supported catalyst. COMSOL includes a tool which can generate a 1-D plot from a 2-D geometry called "cut-line 2-D". The data selection will then be utilized to generate a line plot. A similar method was used in the "CCVD of GaAs" model performed by COMSOL. The generation of carbon at the surface will then help to understand the bottom-up approach for Carbon Nanotube Synthesis using Catalytic Chemical Vapor Deposition. This will help to make the process of experimentation more efficient since an accurate simulation can be referred to.

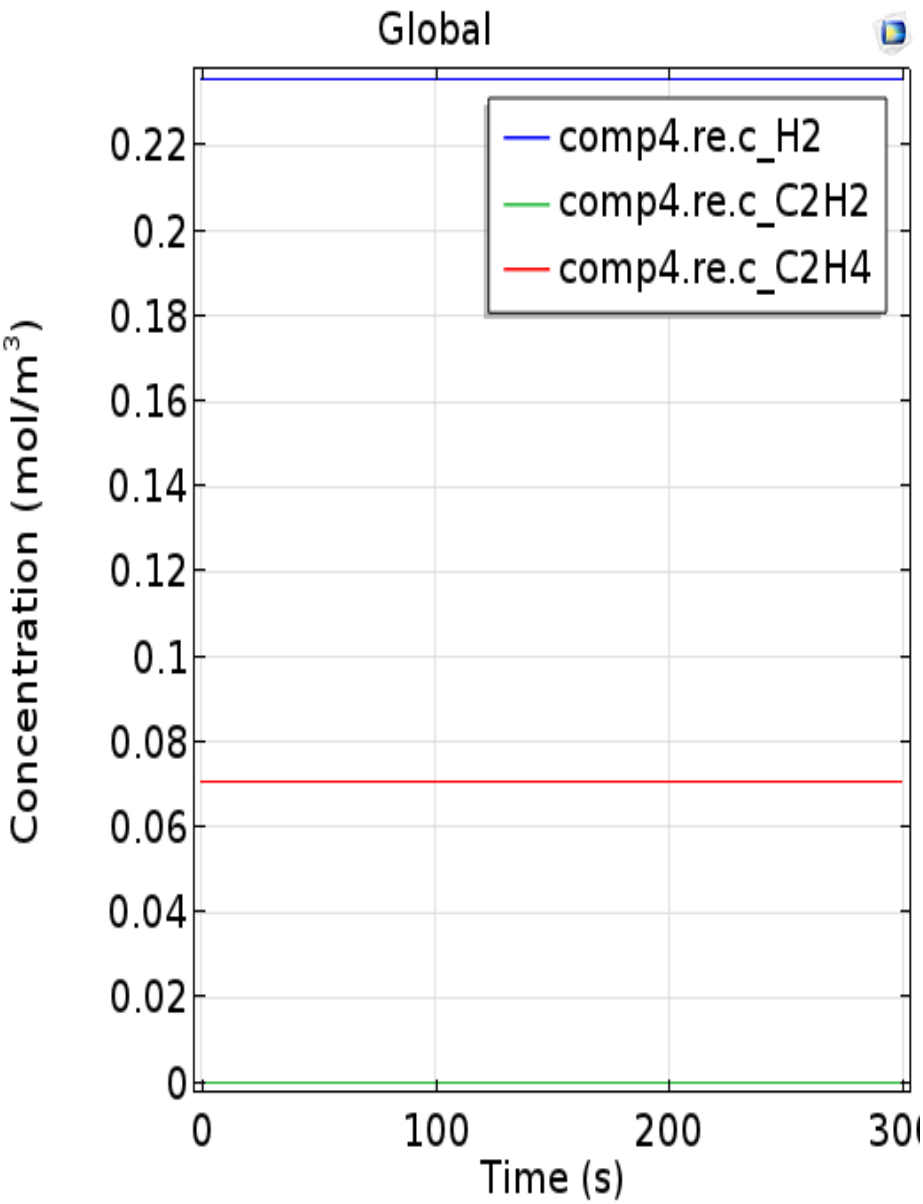

Figure 8.1: Concentrations using Troe Form after 300s in 0-D Batch Reactor Simulation.

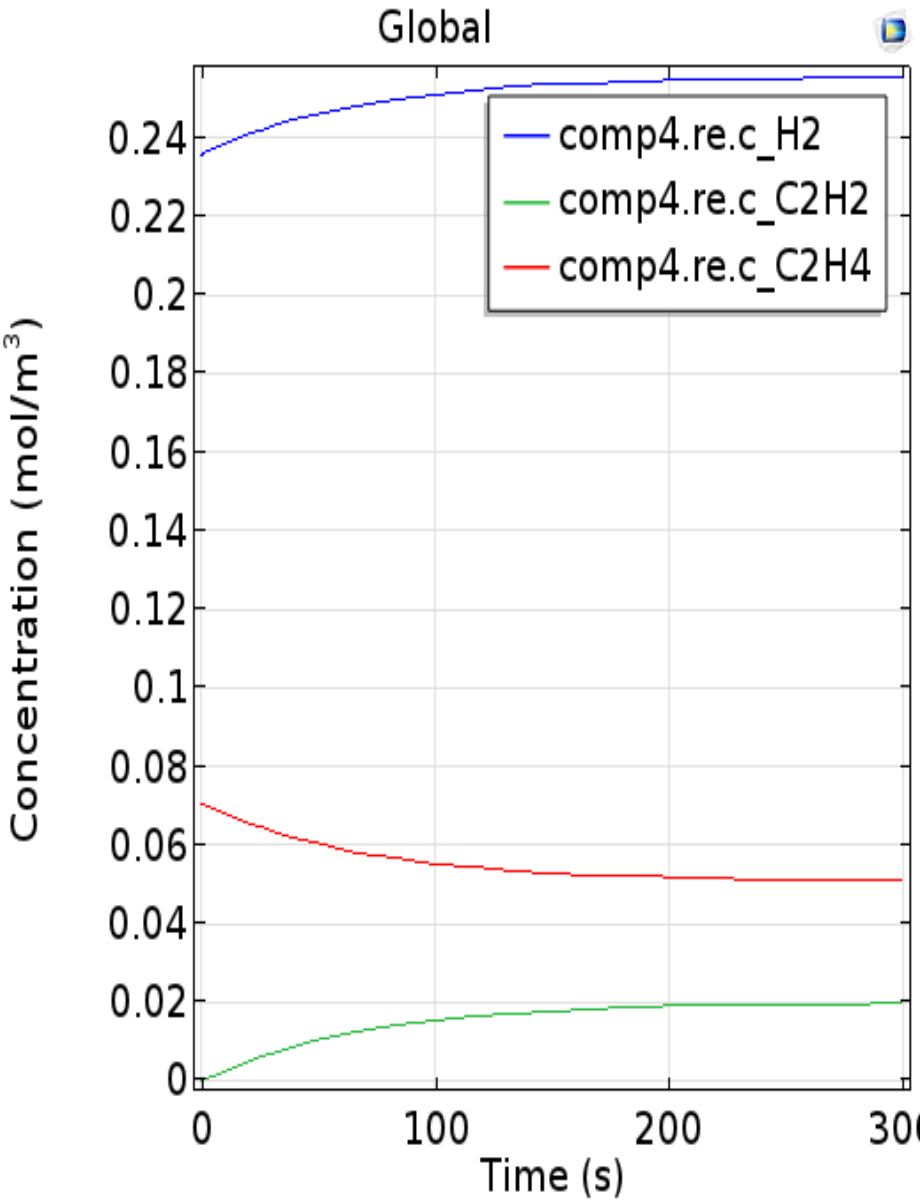

Figure 8.2: Concentrations using Arrhenius Form after 300s in 0-D Batch Reactor simulation.

$2H + Ar = H_2 + Ar$
$2H + H_2 = 2H_2$
$H + CH = C + H_2$
$H + CH_2(+Ar) = CH_3(+Ar)$
$H + CH_3(+Ar) = CH_4(+Ar)$
$H + CH_4 = CH_3 + H_2$
$H + C_2H(+Ar) = C_2H_2(+Ar)$
$H + C_2H_2(+Ar) = C_2H_3(+Ar)$
$H + C_2H_3(+Ar) = C_2H_4(+Ar)$
$H + C_2H_3 = H_2 + C_2H_2$
$H + C_2H_4(+Ar) = C_2H_5(+Ar)$
$H + C_2H_4 = H_2 + C_2H_3$
$H + C_2H_5(+Ar) = C_2H_6(+Ar)$
$H + C_2H_5 = H_2 + C_2H_4$
$C + CH_2 = H + C_2H$
$C + CH_3 = H + C_2H_2$
$CH + H_2 = H + CH_2$
$CH + CH_2 = H + C_2H_2$
$CH + CH_3 = H + C_2H_3$
$CH + CH_4 = H + C_2H_4$
$CH_2 + H_2 = H + CH_3$
$2CH_2 = H_2 + C_2H_2$
$CH_2 + CH_3 = H + C_2H_4$
$CH_2 + CH_4 = 2CH_3$
$2CH_3(+Ar) = C_2H_6(+Ar)$
$2CH_3 = H + C_2H_5$
$CH_3 + C_2H_4 = C_2H_3 + CH_4$
$CH_3 + C_2H_6 = C_2H_5 + CH_4$
$C_2H + H_2 = H + C_2H_2$
$C_2H_4(+Ar) = H_2 + C_2H_2(+Ar)$
$CH + H_2(+Ar) = CH_3(+Ar)$
$CH_2 + CH_2 = 2H + C_2H_2$

Table 8.2: Reactions added in from GRI-Mech 3.0

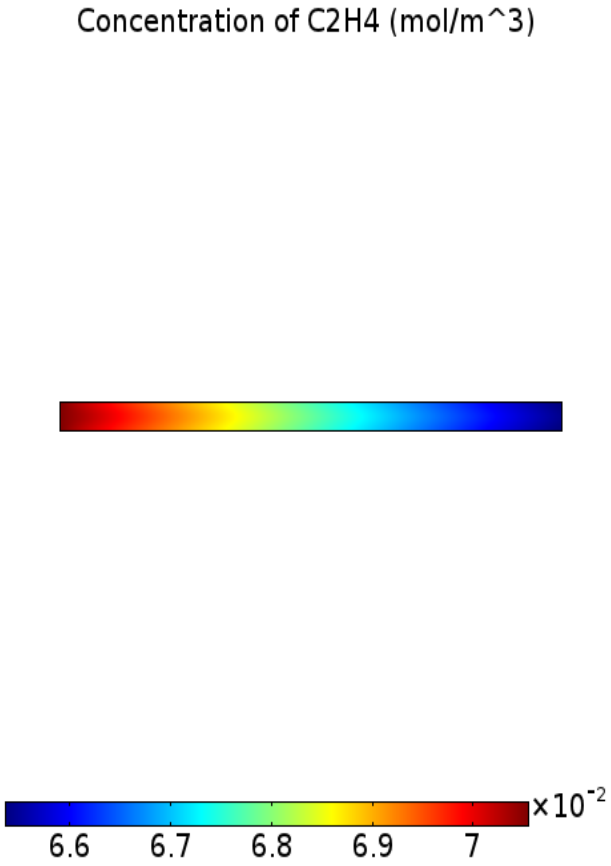

Figure 8.3: Concentration of C_2H_4 after implementing the C_2H_4 decomposition reaction. The range is from 0.06537 to 0.07055 $[\frac{mol}{m^3}]$.

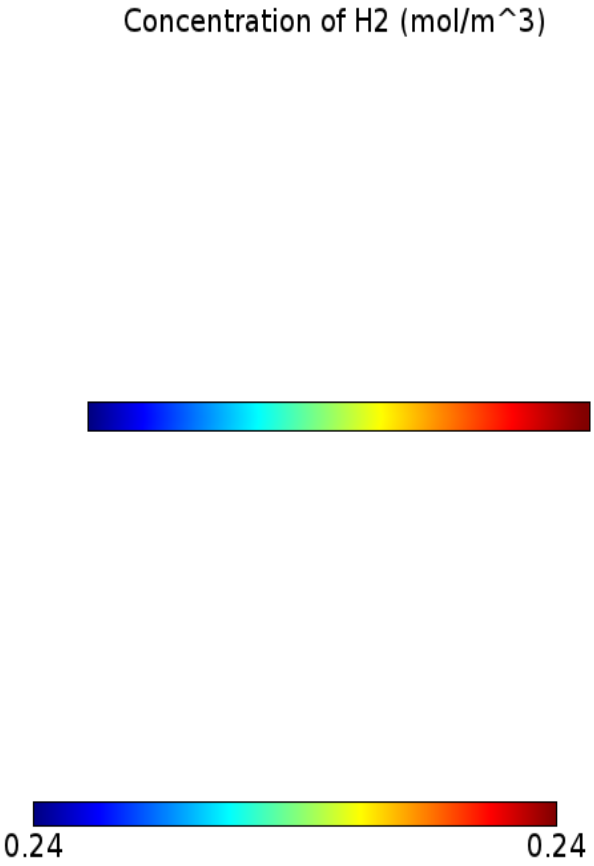

Figure 8.4: Concentration of H_2 from the C_2H_4 decomposition reaction. The range is from 0.23578 to 0.24085 $[\frac{mol}{m^3}]$

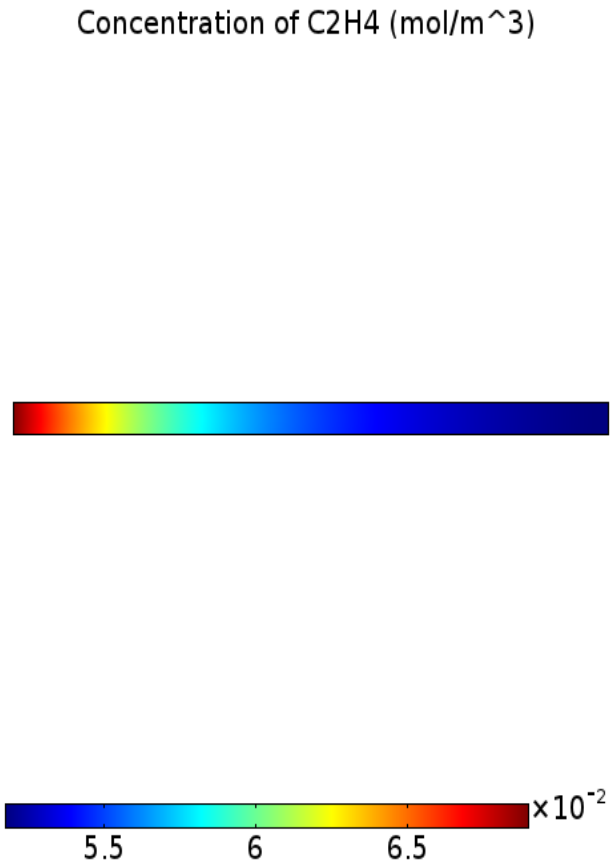

Figure 8.5: Concentration of C_2H_4 after dropping inlet and initial velocities by a factor of 10. The range is from 0.05173 to 0.06901 $[\frac{mol}{m^3}]$. One can see right away that the minimum concentration here matches the equilibrium concentration from the 0-D model much more closely.

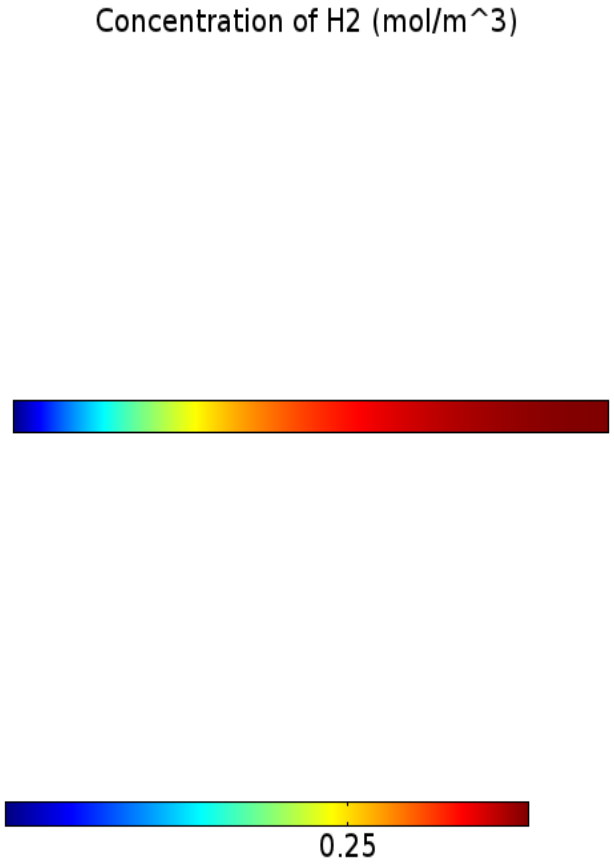

Figure 8.6: Concentration of H_2 after dropping the initial and inlet velocities by a factor of 10. We see that the maximum concentration here is approximately 0.25452 $[\frac{mol}{m^3}]$ which is much more similar to the theoretical equilibrium calculations.

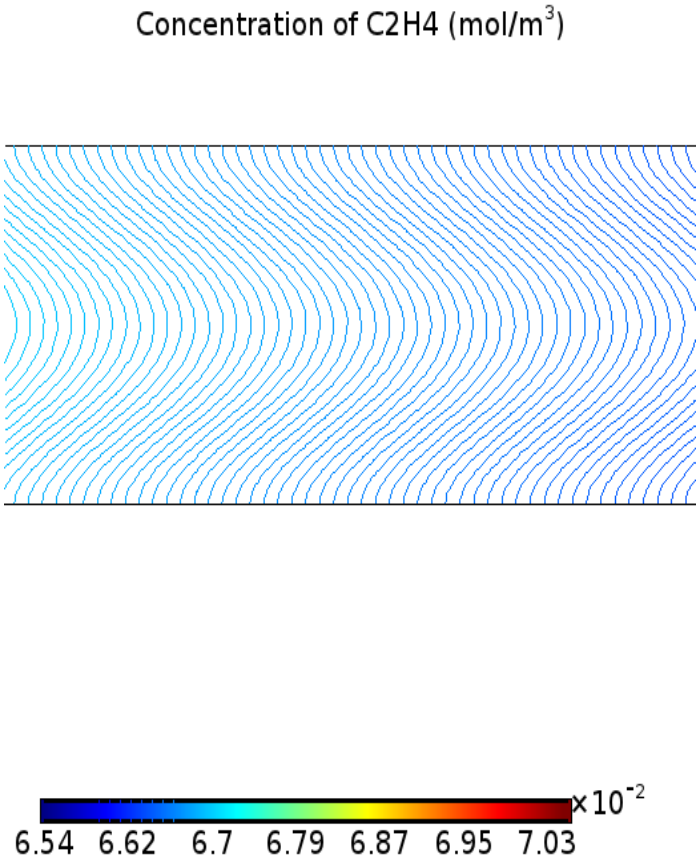

Figure 8.7: Contour plot of concentration of C_2H_4. The plot displays lines of equal concentration. When one chooses where a line intersects a boundary and follows a straight line to the next boundary, the same concentration will be on either surface (as expected). However, along the same line one notices that an intersection will be made with a contour line of lower concentration. As one will see later, the velocity increases from 0 m/s at the surface to a higher value along the centerline. In accordance with the hypothesis, a lower concentration occurs where the lower velocity occurs and the higher concentration occurs when there is a higher velocity.

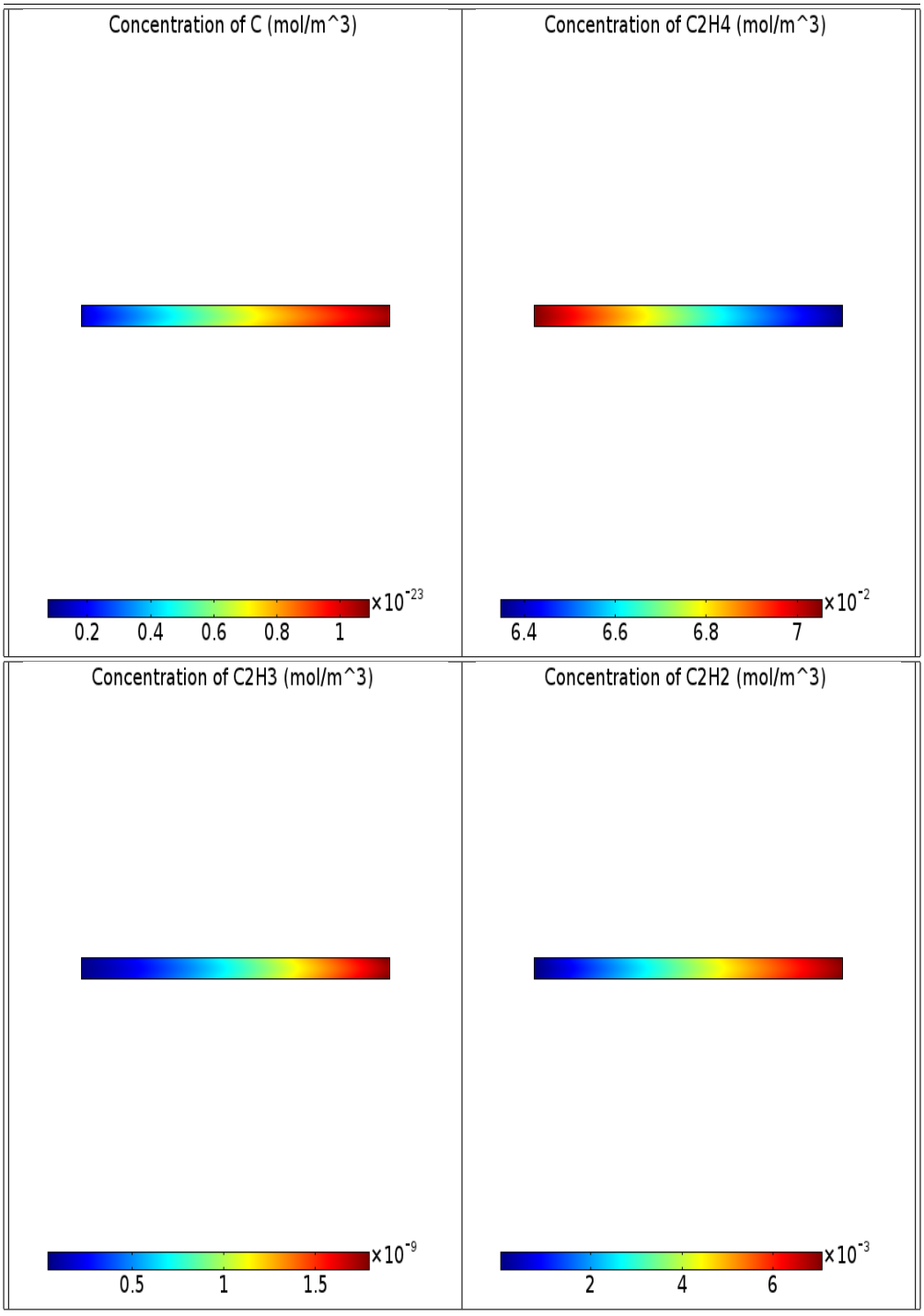
Concentration of C (mol/m^3)
×10^-23
0.2
0.4
0.6
0.8
1
Concentration of C2H4 (mol/m^3)
×10^-2
6.4
6.6
6.8
7
Concentration of C2H3 (mol/m^3)
×10^-9
0.5
1
1.5
Concentration of C2H2 (mol/m^3)
×10^-3
2
4
6

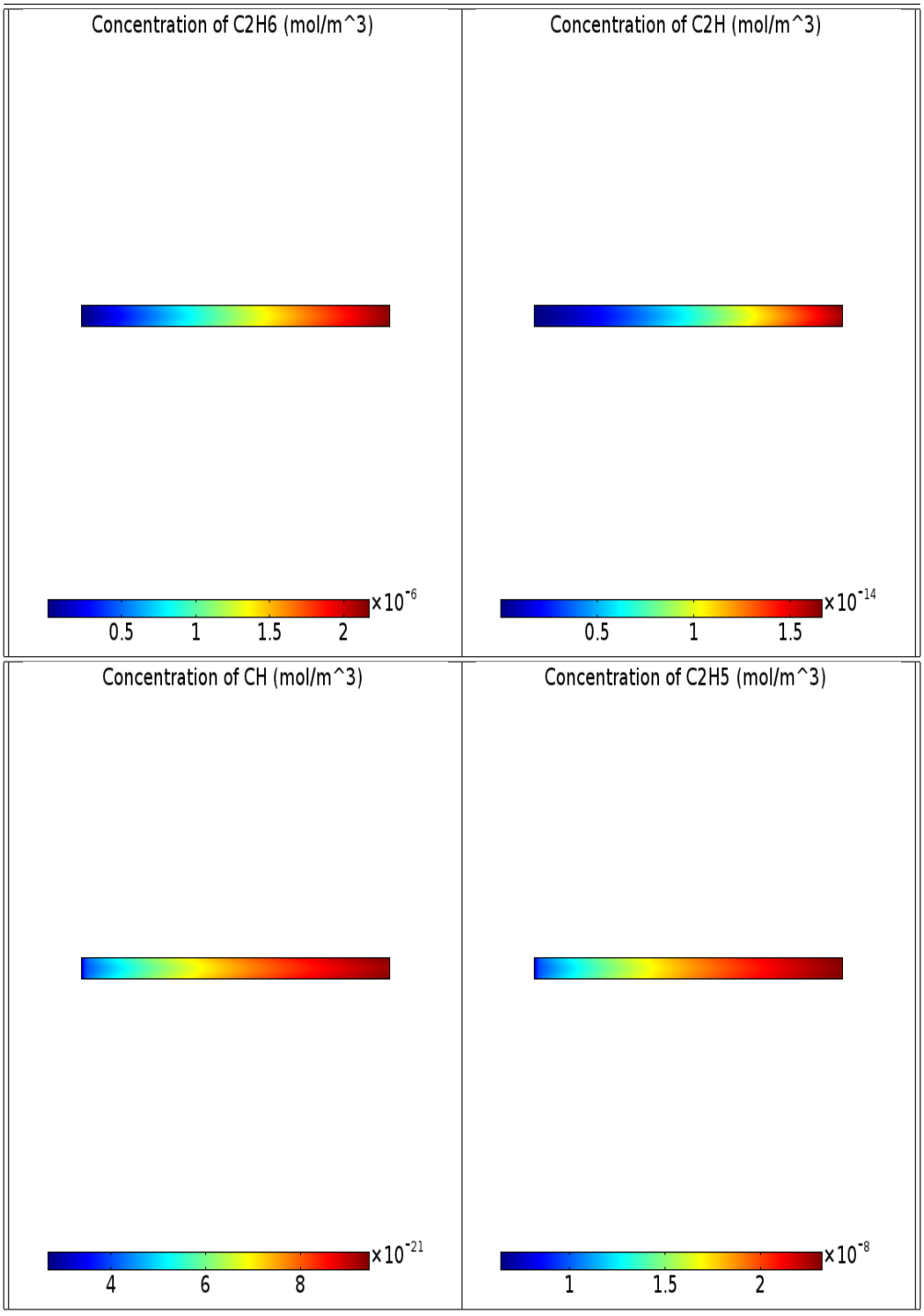
Concentration of C2H6 (mol/m^3)
×10^-6
0.5
1
1.5
2
Concentration of C2H (mol/m^3)
×10^-14
0.5
1
1.5
Concentration of CH (mol/m^3)
×10^-21
4
6
8
Concentration of C2H5 (mol/m^3)
×10^-8
1
1.5
2

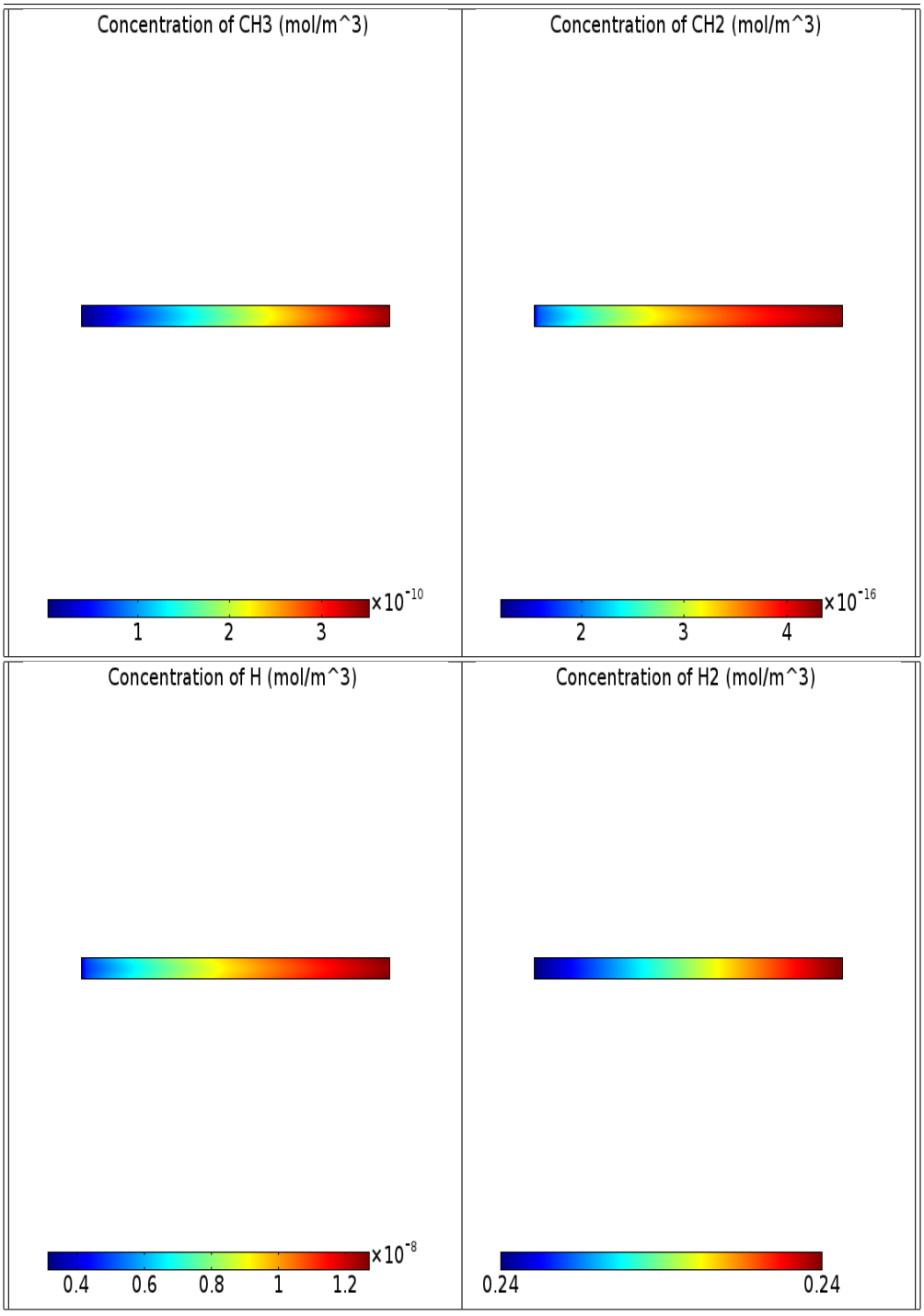
Concentration of CH3 (mol/m^3)
×10^-10
1
2
3
Concentration of CH2 (mol/m^3)
×10^-16
2
3
4
Concentration of H (mol/m^3)
×10^-8
0.4
0.6
0.8
1
1.2
Concentration of H2 (mol/m^3)
0.24
0.24

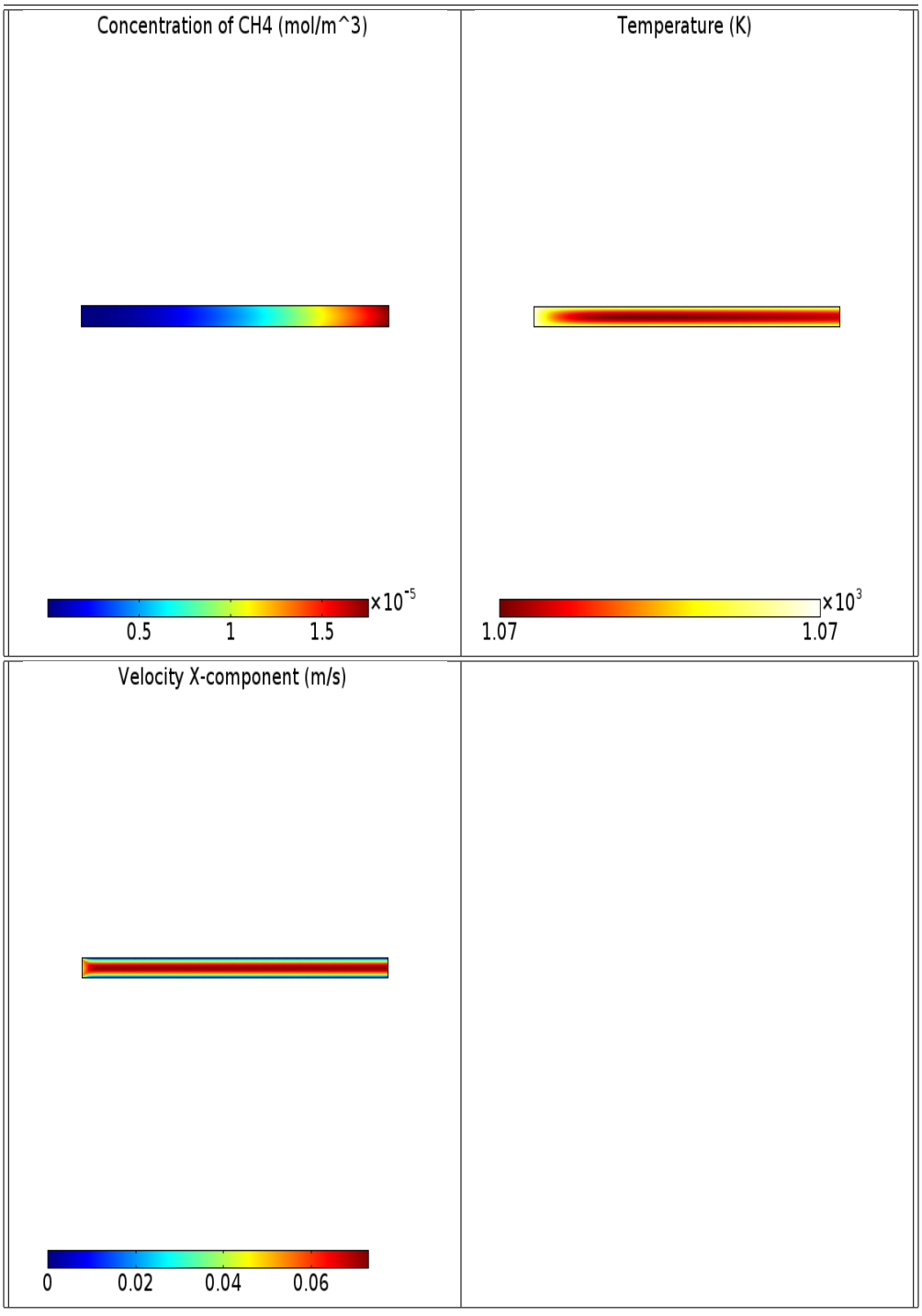

Figure 8.8: Concentration, temperature, and velocity profiles after including the complete set of GRI-Mech 3.0 reactions.

Chapter 9

Conclusion

The end goal of the studies described in this text is to develop a complete gas-phase mechanism, include substrate geometry, and involve surface reactions such that a time-dependent analysis will show the details of carbon formation at the substrate's surface. In this paper, a break down of the process for optimization of the model from time-dependency to steady-state was displayed. Verification of results using 0-D analysis allowed for the understanding of the higher dimensional studies. Specifically, beginning with the ethylene decomposition reaction, reaction direction was analyzed through time-dependent plots of reaction rate. This displayed the effect initial concentrations and rate constants would have on concentration profiles. This simple, yet effective, approach aided in the verification of higher dimensional results.

Although complications arose when attempting to develop a 2-D time-dependent model, plots of concentrations for ethylene, acetylene, and velocity established a basis for the development of the steady-state approach. Within the time-dependent analysis, implementation of step-functions and "eps^2" improved convergence of various reactions. However, due to the introduction of many reactions, it was determined that optimization of the numerical method parameters, as well as meshing, was not established. As previously stated, convergence would be inconsistent and it was observed that the concentrations of species would become negative.

Before continuing with a more in-depth time-dependent model, a 2-D steady-state model was generated using similar boundary conditions from the time-dependent study. In this case, step functions were not necessary, but the "eps^2" constant was incorporated such that negative concentrations were avoided. In order to optimize the mesh size, a 1-D study was performed in order to determine whether or not the standard "physics-controlled" settings would eliminate any inconsistent, negative concentrations. It was observed that a "user defined" mesh was needed.

After implementation of a mesh size of approximately 0.00099[m], results were more consistent. However, within some of the concentration plots negative values remained. Optimization of the BDF numerical method through varying relative tolerance and a segregated solver greatly improved convergence and numerical stability.

Before continuing with an extensive list of reactions to include, verification of results was performed through the utilization of a 0-D study in comparison to ICE table results. It was determined that the projected equilibrium concentrations did not match up with the results in 0-D using Troe Form kinetics. High pressure rate limits for relevant reactions were then implemented.

This allowed for the complete implementation of nearly 32 gas-phase reactions directly from the GRI-Mech 3.0 resource, excluding reactions including singlet-state species. There were a couple of reactions which were not able to be implemented due to convergence errors arising. Studies were performed such that the reaction set was decreased, allowing for testing to determine whether or not the issue was arising numerically or from user error. Reduction in the list led to convergence, which implied that numerical instability was occurring due to the reaction mechanism not being reduced.

Plots of thirteen different species' concentrations were generated with an exclusion of the substrate, to allow for convergence. Gas-phase velocity and temperature were also plotted in order to look for consistencies. A laminar profile for the velocity, similar to the time-dependent studies, was observed. Most notably, contour plots of the concentration for ethylene were generated in order to observe the effect of temperature and velocity on concentration. A decrease in velocity increased cracking efficiency, such that a parabolic curvature in the contour plots was determined from the reactor centerline to the reactor surfaces. The lower velocity also corresponded to higher temperatures at the reactor surface, which also contributed to more efficient ethylene cracking.

At 800C, with an inlet velocity defined using volumetric flowrates for ethylene, argon, and molecular hydrogen as 30, 470, and 100 in SCCM respectively, the concentration of interest for amorphous carbon was established. In a comparative study using CHEMKIN, for a batch reactor, the gas-phase concentration of a-C was projected to be approximately $10^{-22}[mol/m^3]$. Within the 2-D steady-state study, the a-C concentration was determined to be on the order of approximately $10^{-23}[mol/m^3]$. This result was impacting because it displays that at the current inflow velocity at temperature, the production of a-C is essentially null.

Explanations for the particular concentration of a-C include the obvious lower

temperature for decomposition. Studies at higher temperatures (approximately 900C) which displayed a much more efficient production of a-C. Hence, it is possible that if the reactor temperature was increase to a much larger value then a-C may be significant in CNT production. Lastly, since surface reactions have not been included, an overall production of a-C is not being observed. It is possible for a-C to deposit on the reactor's surface, so with an introduction of said reactions one may notice a larger concentration of amorphous carbon. It is currently unknown how large the contribution of a-C would be to cap formation and the thought is that active gas-phase species will promote more efficient cap formation. An inclusion of surface reactions on the substrate will answer this question. Once a complete reduction of the gas-phase mechanism takes place, then the substrate can be reincorporated for such an analysis.

Bibliography

[1] Rockett A. *"The materials science of semiconductors"*.

[2] Negrut D., Jay L.O., and Khude N. "A discussion of low-order numerical integration formulas for rigid and flexible multibody dynamics". *Journal of Computational and Nonlinear Dynamics*, 4(2), 2009.

[3] Littmarck F. "Modeling chemical reactions: 3D model of a monolithic reactor". https://www.comsol.com/blogs/modeling-chemical-reactions-3d-model-of-a-monolith-reactor/.

[4] Smith G.P., Golden D.M., Frenklach M., Moriarty N.W., Eiteneer B., Goldenberg M., Bowman C.T., Hanson R.K., Song S., Gardiner W.C. Jr., Lissianski V.V., and Qin Z. "GRI-Mech 3.0". http://www.me.berkeley.edu/gri_mech/.

[5] Hinkov I., Farhat S., Lungu C.P., Gicquel A., Silva F., Mesbahi A., and Anghel A. "Microwave Plasma Enhanced Chemical Vapor Deposition of Carbon Nanotubes". *Journal of Surface Engineered Materials and Advanced Technology*, 4(04), 2014. pg. 196.

[6] Tessonnier J.P. and Su D.S. "Recent progress on the growth mechanism of carbon nanotubes: a review". *ChemSusChem*, 4(7), 2011. pg. 824-847.

[7] Gulas M., Cojocaru C.S., Le Normand F., and Farhat S. "An Investigation of the Plasma Composition in Plasma-Enhanced Hot Filament Catalytic Chemical Vapor Deposition of Carbon Nanotubes". *Plasma Chemistry and Plasma Processing*, 28(1), 2008. pg. 123-146.

[8] COMSOL Multiphysics. "Chemical vapor deposition of Gallium Arsenide". http://www.comsol.com/model/download/222541/models.chem.gaas_cvd.pdf.

[9] Janardhanan V.M. and Deutschmann O. "CFD analysis of a solid oxide fuel cell with internal reforming: Coupled interactions of transport, heterogeneous

catalysis and electrochemical processes". *Journal of Power Sources*, 162(2), 2006. pg. 1192-1202.